ACS EARTH AND SPACE CHEMISTRY

http://pubs.acs.org/journal/aesccq

Article

Origins of Organic Matter, Paleoenvironment, and Hydrocarbon Potential of the Carboniferous Source Rocks from Shibei Sag, Junggar Basin, NW China

Xue Chen, Xiao Jin, Xinjian Zhu, Ningning Zhong, and Zhihuan Zhang*

Cite This: *ACS Earth Space Chem.* 2023, 7, 92−109

Read Online

ACCESS | Metrics & More | Article Recommendations | Supporting Information

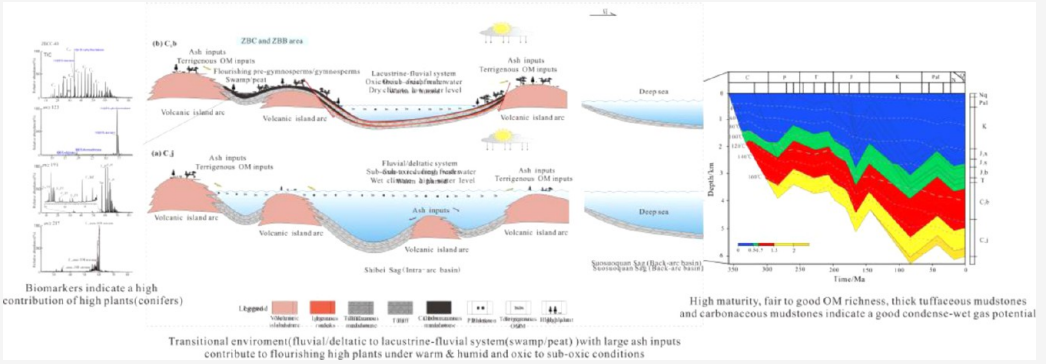

ABSTRACT: The organic-rich sediments of the Carboniferous in the Shibei Sag, Junggar Basin, China are potential source rocks with good hydrocarbon generation conditions for oil and gas exploration. Thus, it is meaningful to analyze their geochemical characteristics, including the hydrocarbon generation potential, genetic types of kerogen, thermal maturity, the origin of organic matter (OM), and sedimentary environment. The results reveal that the Carboniferous source rocks have fair to excellent hydrocarbon generation potential. They are mainly gas-prone with type III-IIkerogens. Random vitrinite reflectance (Rr) of the studied samples ranges from 0.63 to 1.04%, suggesting a primarily mature stage, which is also supported by the maturity-related hopane and sterane ratios. Stable carbon isotopic compositions, organic petrological macerals, and biomarker characteristics all indicate a predominant higher plant input. Abundant bicyclic sesquiterpenoids and diterpenoid biomarkers in the studied samples suggest the conifer inputs. In particular, high amounts of phyllocladanes, retene, and kauranes suggest the contribution of gymnosperms, pre-gymnosperms, pteridophytes, or bryophytes in swamps. From the early Carboniferous to the late Carboniferous, the environment became more oxic, the water level dropped, and higher plants flourished. Based on the abovementioned results, the Carboniferous source rocks were likely to be deposited in a transitional environment under lacustrine-fluvial conditions. Specifically, source rocks from the Batamayineishan Formation were deposited in a peat environment during the interval of the volcano eruptions. Considering the quantity and maturity of OM and their large thickness, the Carboniferous sediments have a good petroleum exploration potential.

KEYWORDS: *source rock, biomarkers, stable carbon isotopes, organic geochemistry, Carboniferous, Junggar Basin*

1. INTRODUCTION

The Junggar Basin, situated in northwestern China, has high hydrocarbon potential.[1−3] More than 30 volcanic oil and gas reservoirs have been discovered in the northwestern margin, leading to an increasing attention for the volcanic oil and gas reservoirs since the 1950s. For example, the Shixi volcanic reservoir, which was discovered in the basin abdomen in 1994, was the largest buried hill reservoir of volcanic rocks in China, and it was built up quickly with a production capacity of 1 million tons, which greatly promoted the development of volcanic rock exploration, for example, Kelameili gas field, Wucaiwan gas field, and Chepaizi oil field.[4,5] The exploration of natural gas and oil shows that the Carboniferous source rocks have become one of the important gas-generating source rocks in the Junggar Basin. Some researchers proposed that the coal-bearing source rocks have become the main content for gas fields in the eastern Junggar Basin.[6−8] Wang et al.[9] conducted a detailed analysis and evaluation of the Carboniferous source rocks in the Ludong−Wucaiwan area, Junggar Basin. Zhang and

Received: August 9, 2022
Revised: November 27, 2022
Accepted: November 28, 2022
Published: December 12, 2022

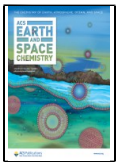

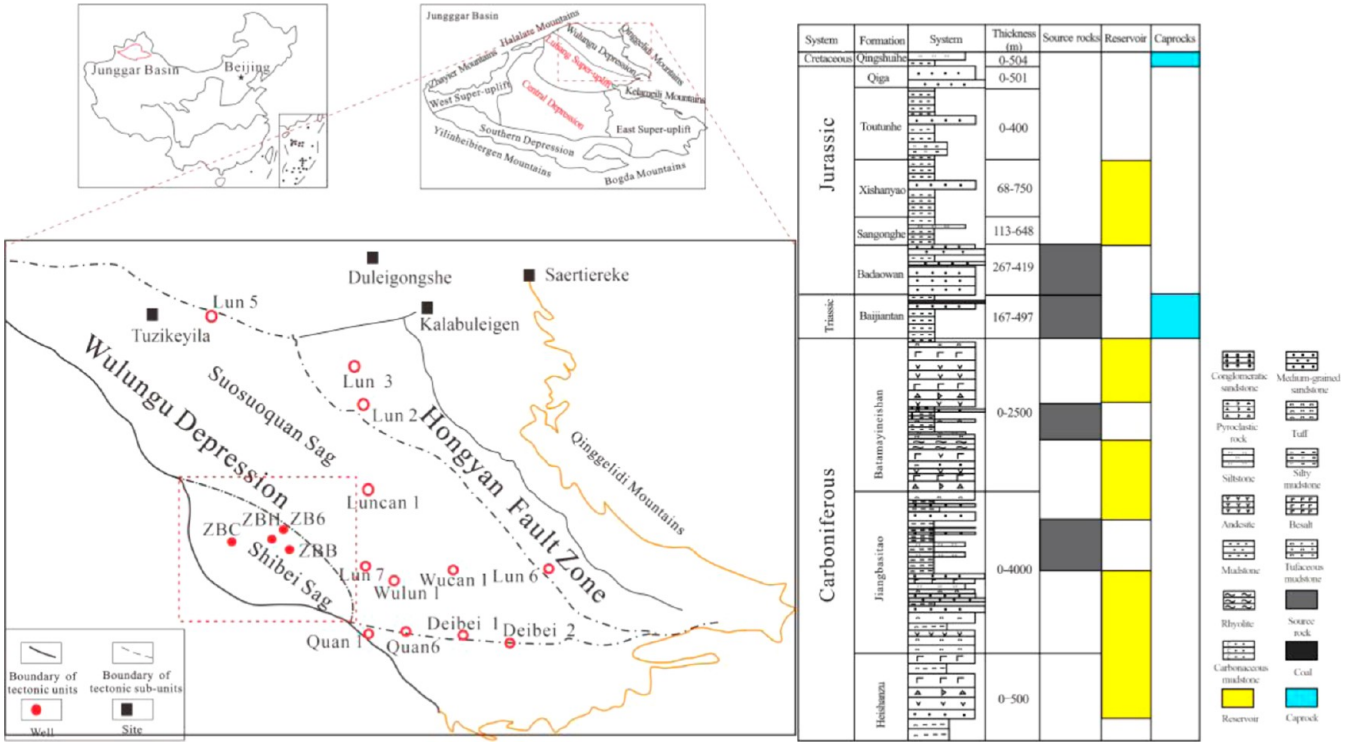

Figure 1. Location of the study area, generalized stratigraphy, and the main source rocks, reservoirs, and caprocks in the northern Junggar Basin.

Li et al.[10,11] demonstrated that the Carboniferous sediments in the Ludong-Wucaiwan area were the main gas source rocks for the Kelameili and Wucaiwan gas field. Similarly, Yu et al.[12] investigated the organic geochemistry of the Carboniferous source rocks and revealed that the oils and gases of the Kelameili gas field in the eastern Junggar Basin were generated from the source rocks of the Dishuiquan Formation (C_1d). Moreover, Gong et al.[13] proposed that the Carboniferous source rocks in the southeastern Junggar Basin were primarily gas-prone which were deposited in an oxidized−suboxized environment, and the origins of the natural gases in the southeastern Junggar Basin were the highly mature coaly source rocks of the Carboniferous from the Fukang Depression. However, only a few studies on the paleoenvironment and environmental evolution of the Carboniferous were conducted in the northwestern Junggar Basin.

Biomarkers are stable compounds that can be preserved in the OM over geological time. They have many different biological origins, and some biomarkers may be related to a specific source. They are useful indicators that can provide significant information on the biological origins and depositional conditions of the OM, such as climate or redox.[14] A detailed geochemical analysis of source rocks for the palaeovegetation, the palaeoenvironment, and hydrocarbon potentials can contribute to the petroleum exploration.

In this study, we select the Shibei Sag situated in the northeastern Junggar Basin as our study area because of its high hydrocarbon potentials. However, the complex tectonic evolution and intensive volcanic activity, which prevails in the Carboniferous, obscure the understanding of sediment body and the distribution of hydrocarbon, making it difficult to explore. Until now, there is no detailed analysis of organic geochemical characteristics and the depositional environment of the Carboniferous sediments in the Shibei Sag, which may hinder its exploration. Two aims of this study can be summarized as follows: first, to provide a comprehensive understanding of the hydrocarbon potential, the genetic type of kerogen, organic matter (OM) source, and thermal maturity of the potential source rocks in the Carboniferous and, second, to reveal its sedimentary conditions and evolution.

2. GEOLOGICAL SETTING

The Junggar Basin, superimposed by intracontinental and foreland basins, is a large-scale composite basin. The Wulungu Depression is a first-order geological unit in the north of the Junggar basin, trending NW-SE like a rhombus, and it is composed of the Suosuoquan Sag and the Hongyan Fault Zone and the Shibei Sag (Figure 1). The Shibei Sag is a residual sag of the Luliang Uplift. There were four periods of tectonic events in the Junggar Basin, including the Hercynian, the Indosinian, the Yanshan, and the Himalaya.[15,16] The Carboniferous, Triassic, Jurassic, and Cretaceous strata were deposited in the study area, while the Permian, low-middle Triassic, and Cenozoic strata were absent, caused by the Hercynian and Indosinian movement. The Junggar Basin existed as an ocean facies during the early Carboniferous but as a continent facies during the late Carboniferous. Residual oceans (sea), back-arc basin, intra-arc basin, marine rift, and continental rift provide favorable conditions for the accumulation of OM. In the early Carboniferous, there were some volcanic arcs distributing along the Luliang—Kelameili field, among which were Shixi, Shibei, and Dishuiquan intra-arc sags. In the late Carboniferous, the pattern of south-ocean versus north-continent was formed, and the continental rift facies with a series of volcanic clastic rocks, source rocks, and volcaniclastic rocks developed in the northeastern Junggar Basin. Frequent volcanic activities led to the deposition of magmatite rocks and sedimentary rocks in the Carboniferous. Strata in the Carboniferous were mainly composed of tuffaceous mudstone, carbonaceous mudstone, and volcanic rocks. It was obvious that volcanic activities were common in the Junggar Basin, and these volcanic rocks and

https://doi.org/10.1021/acsearthspacechem.2c00241
ACS Earth Space Chem. 2023, 7, 92−109

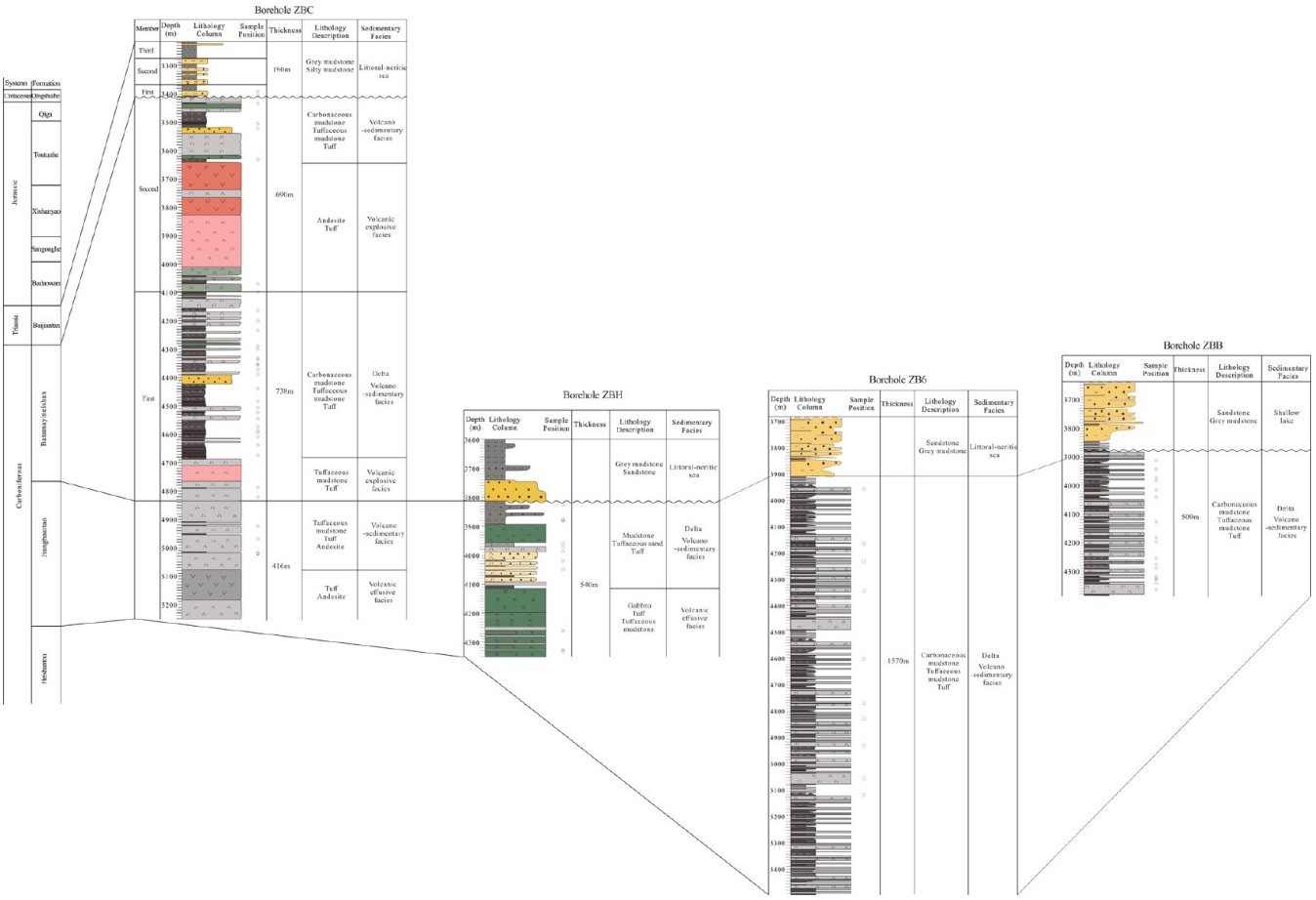

Figure 2. Columnar section of the well ZBC, ZBB, ZBL, and ZBH, showing the characteristics of sediments and positions of the studied samples in the Carboniferous.

tuffaceous/carbonaceous mudstones were a good combination of reservoirs and source rocks in the Shibei Sag. However, the organic geochemistry and depositional environment of the Carboniferous sediments in the Shibei Sag have not been well documented.

3. SAMPLING AND METHODS

The samples were collected from the Jiangbasitao Formation (C_1j) and the Batamayineishan Formation (C_2b) of four wells (ZBB, ZBC, ZBL, and ZBH shown in Figure 1) in the Shibei Sag. The samples were crushed and sieved under 100-mesh in order to conduct the total organic carbon (TOC), Rock-Eval pyrolysis, carbon isotope of kerogen, and extraction experiments, and the analytical results are provided in the Supporting Information.

3.1. Total Organic Carbon (TOC) Measurement and Rock-Eval Pyrolysis Analysis. The TOC analysis of 65 powdered samples was conducted by the Leco CS-230 apparatus after acid treatment which aims to remove carbonate minerals. Then, the organic carbon of the samples was completely oxidized into carbon dioxide by heating to 900 °C. Then, generated carbon dioxide can be used to estimate the TOC contents.

The rock pyrolysis data were obtained through the OGE-II workstation according to a standard procedure (GB/T18602-2001) by heating the samples in a helium atmosphere. The rock pyrolysis data included the temperature of maximum pyrolysis yield (T_{max} °C), free hydrocarbon values (S_1-mg HC/g rock), and remanent hydrocarbon values (S_2-mg HC/g rock).

3.2. Solvent Extraction, Fractionation, and Gas Chromatography−Mass Spectrometry. The extractable organic matter (EOM) was extracted in the Soxhlet with a dichloromethane/methanol mixture (93:7 v/v) for 72 h. After extraction, the extracted samples were separated into saturated hydrocarbons, aromatic hydrocarbons, resin, and asphaltene by dissolving and rinsing.

The gas chromatography−mass spectrometry (GC−MS) analysis of the saturated hydrocarbon and aromatic hydrocarbon fractions was conducted on an Agilent 5975i mass spectrometer, coupled with an Agilent 6890 gas chromatography instrument equipped with an HP-5MS column (60 m × 0.25 mm i.d. and 0.25 μm film thickness), and ultrahigh purity helium was used as the carrier gas at a flow rate of 1 mL/min (70 eV ionization energy). Moreover, the temperature of the sample inlet is maintained at 300 °C. The temperature of the GC oven analyzing saturated hydrocarbons was set at 50 °C for 1 min, then gradually increased to 310 °C at a rate of 3 °C/min, and held at 310 °C for 25 min, while the GC oven temperature analyzing aromatic hydrocarbon was initially set to 80 °C, gradually increased to 310 °C at 3 °C/min, and kept at 310 °C for 20 min. MS was scanned from m/z 50 to 550 using both the selective ion monitoring (SIM) mode and the total ion current (TIC) to analyze the distributions of the aliphatic and aromatic hydrocarbons.

https://doi.org/10.1021/acsearthspacechem.2c00241
ACS Earth Space Chem. 2023, 7, 92−109

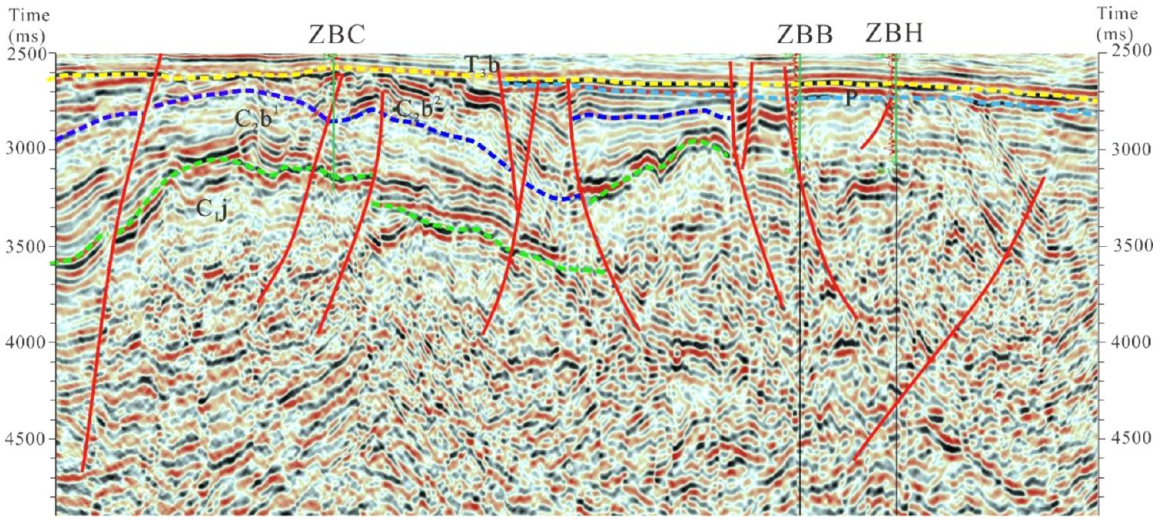

Figure 3. Time section of the ZBC, ZBB, and ZBH borehole in the study area.

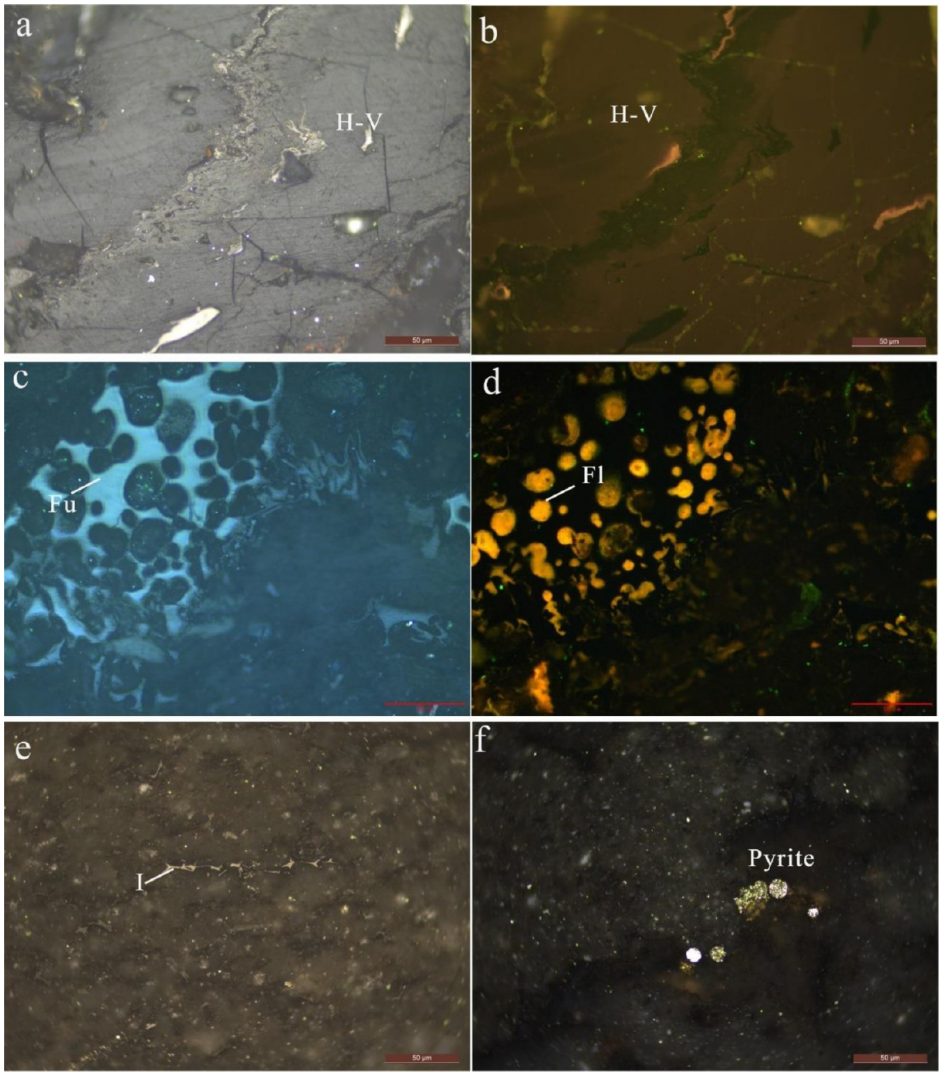

Figure 4. Representative maceral components, including hydrocarbon-rich vitrinite (H-V), fusinite (Fu), fluorinite (Fl), inertinite (I), and pyrite of the Carboniferous source rocks from the Shibei area, Junggar Basin. Photographs (a,b) and (c,d) are in the same area under reflected light and fluorescent light, respectively, ZBC; (e,f) under reflected light, ZBH.

3.3. Organic Carbon Isotope Analysis. The stable carbon isotope ($\delta^{13}C$) values of chloroform bitumen"A", saturated fraction, aromatic fraction, resin, and asphaltene were measured on the Thermofisher Flash 2000 EA-Mat 253 isotope-ratio mass

https://doi.org/10.1021/acsearthspacechem.2c00241
ACS Earth Space Chem. 2023, 7, 92−109

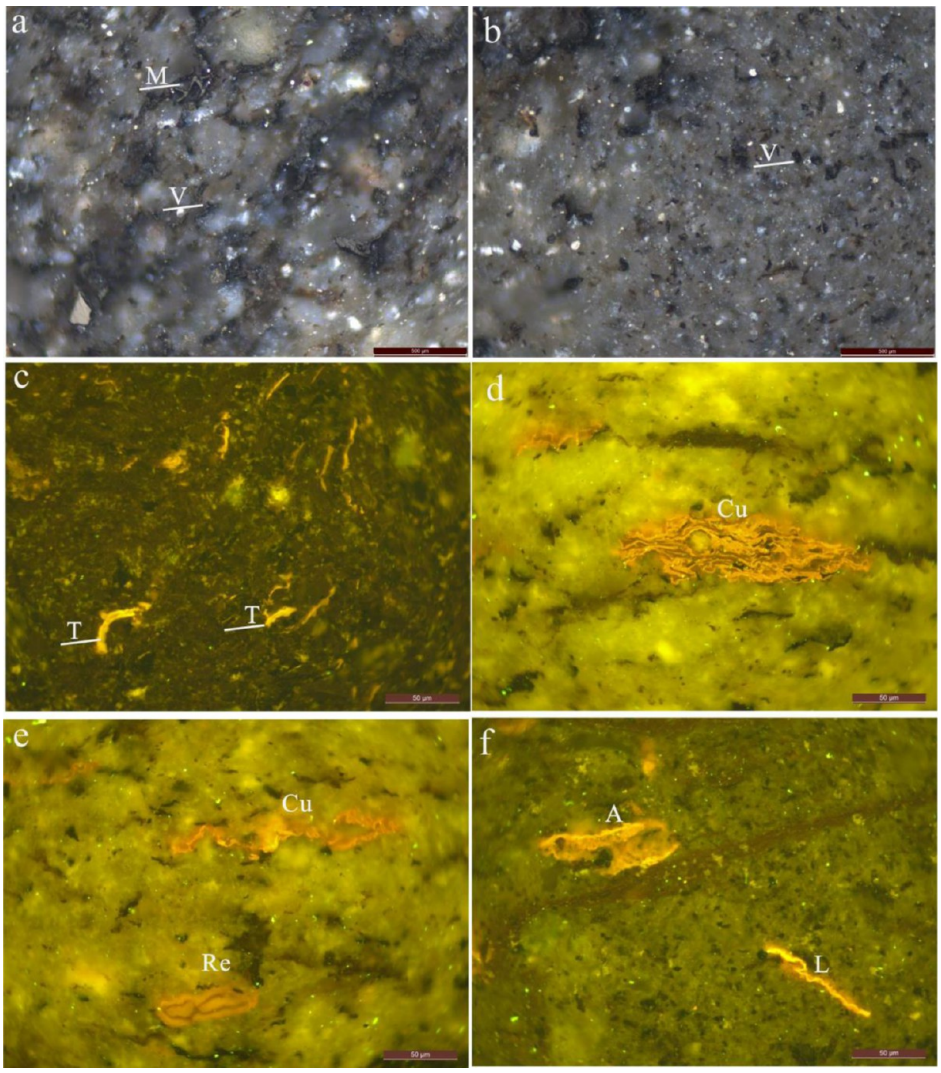

Figure 5. Typical macerals, including micrinite (M), vitrodetrinite (V), alginite (A), telalginite (T), lamalginite (L), resinite (Re), and cutinite (Cu) of the Carboniferous source rocks from the Shibei area, Junggar Basin. (a,b) Under reflected light, ZBL; (c−f) under fluorescent light, ZBB.

spectrometer (IRMS). The carrier, combustion, and sweeping gases are ultrahigh purity He, O_2, and He with flows of 100, 250, and 250 mL/min, respectively. Results of $\delta^{13}C$ were reported relative to the Pee Dee Belemnite (PDB) standard.

3.4. Analysis of Macerals. The organic maceral composition analysis was conducted on a Leica microscope under the reflected white and fluorescent light. The measurements of vitrinite reflectance (Ro) were performed under reflected light at 546 nm (1.518 refractive index oil) with oil immersion. At least 30 vitrinite particles were measured in each sample. Maceral percentages are based on visual estimates.

4. RESULTS

4.1. Petrography. Volcanic activities were active during the period of Carboniferous, resulting in a series of volcanic deposits in the northwestern Junggar Basin, including tuff, volcanic breccia, andesite, tuffaceous mudstone, and so forth. Some studies have proven that volcanism has positive effects on the enrichment of OM.[17] There are also some corresponding source rocks deposited during the interval of the volcano eruptions. The Carboniferous strata are composed of the Batamayineishan Formation (C_2b) and the Jiangbasitao Formation (C_1j) in the Shibei Sag. Unconformable contact always occurs between the Jiangbasitao Formation strata and the Batamayineishan Formation strata. From the section of ZBC-ZBH-ZBL-ZBB (Figures 2 and 3), we can predict that the whole sedimentary sequence is as follows: from volcanic explosive facies, volcanic-sedimentary (delta) facies, and volcanic effusive facies to volcanic-sedimentary (delta) facies in the Jiangbasitao Formation and from volcanic explosive facies to volcanic-sedimentary (delta) facies in the Batamayineishan Formation. Strata deposited during the interval of the volcano eruptions are characterized by the tuff interbedded with tuffaceous mudstone, carbonaceous mudstone, or mudstone. Especially, these volcanism-related mudstones are our targeted source rocks.

4.2. Basic Organic Geochemical Characterization. The Carboniferous source rocks, including mudstone, tuffaceous mudstone, and carbonaceous mudstone, have variable TOC, S_1, and S_2 contents (Table S1 in the Supporting Information). The TOC contents for the samples in the Jiangbasitao Formation span from 0.28 to 18.66 wt %, while that of the Batamayineishan Formation samples span from 0.55 to 29.73 wt %. The carbonaceous mudstones (5.70−29.73 wt %, with an average value of 15.21 wt %) and tuffaceous mudstones (0.46−5.42 wt %, with an average value of 2.87 wt %) have higher TOC values,

https://doi.org/10.1021/acsearthspacechem.2c00241
ACS Earth Space Chem. 2023, 7, 92−109

Table 1. Organic Geochemical Proxies of Study Samples

parameters	sample no.										
	ZBCC-40	ZBCC-21	ZBCC-17	ZBCC-28	ZBCC-33	ZBCC-36	ZBCC-37	ZBB-544	ZBBC-10	ZBBC-11	ZBBC-16
formation	C_2b	C_2b	C_2b	C_2b	C_2b	C_2b	C_1j	C_1j	C_1j	C_1j	C_1j
CPI_{22-32}[a]	1.33	1.35	1	1.1	1.04	1.01	0.97	0.99	1.12	1.11	1.13
TAR	0.43	0.45	0.22	0.11	0.1	0.08	0.08	0.07	0.22	0.26	0.18
Pr/Ph	4.44	4.09	1.25	1.88	1.77	2.18	2.05	1.23	1.67	2.25	3.52
Pr/nC_{17}	1.95	1.74	0.53	0.44	0.45	0.52	0.47	0.41	0.75	0.77	0.68
Ph/nC_{18}	0.31	0.31	0.35	0.19	0.25	0.2	0.2	0.13	0.4	0.28	0.17
$\sum C_{21-}/\sum C_{22+}$	0.71	0.65	1.83	1.85	2.28	1.98	1.98	2.35	1.50	1.29	1.37
Ts/Tm	0.03	13.88	0.23	0.48	0.41	0.34	0.51	0.64	0.17	0.19	0.2
Ts/(Ts + Tm)	0.03	0.93	0.19	0.33	0.29	0.25	0.34	0.39	0.14	0.16	0.16
$C_{31}\alpha\beta$-22S/(22S + 22R)	0.58	0.59	0.57	0.58	0.59	0.57	0.58	0.56	0.58	0.58	0.58
$C_{32}\alpha\beta$-22S/(22S + 22R)	0.58	0.56	0.58	0.58	0.59	0.58	0.58	0.59	0.58	0.59	0.59
gammacerane index (GI)	0	0.3	0.06	0	0	0.14	0.15	0.08	0	0.03	0.03
C_{35}/C_{34} hopane	0.59	0.38	1.21	0.39	0.51	0.43	0.43	0.49	0.4	0.4	0.43
C_{19}/C_{23}TT	2.86	3.18	2.23	4.5	1.74	2.27	1.86	2.33	1.44	1.71	2.42
C_{20}/C_{23}TT	4.84	4.26	1.52	7.95	2.1	2.78	2.56	1.78	1.51	2.19	2.7
$(C_{19} + C_{20})TT/C_{23}TT$	7.7	7.44	3.75	12.46	3.84	5.05	4.42	4.11	2.95	3.9	5.12
$C_{24}TeT/(C_{24}TeT + C_{23}TT)$	0.87	0.88	0.5	0.81	0.64	0.74	0.7	0.77	0.64	0.73	0.76
ETR	2.69	1.52	1.47	1.11	1.53	1.55	1.5	0.28	1.07	1.47	1.74
$C_{24}TeT/C_{26}TT > 1.0$	7.14	9.52	1.96	8.07	5.19	5.87	4.32	4.29	3.87	5.77	6.13
$C_{31}R/C_{30}$	0.52	0.52	0.33	0.28	0.31	0.33	0.32	0.29	0.36	0.35	0.33
ΣTT/Σhopanes	0.02	0.02	0.16	0.21	0.23	0.14	0.2	0.21	0.25	0.05	0.07
$C_{23}TT/C_{30}$ hopane	0.01	0	0.1	0.04	0.12	0.05	0.07	0.08	0.12	0.02	0.02
$C_{29}\alpha\beta/(\alpha\beta + \beta\alpha)$ hopane	0.77	0.77	0.88	0.89	0.89	0.83	0.91	0.87	0.86	0.86	0.87
$C_{30}\alpha\beta/(\alpha\beta + \beta\alpha)$ hopane	0.68	0.68	0.83	0.86	0.86	0.81	0.93	0.86	0.85	0.86	0.86
$C_{29}/C_{30}\alpha\beta$ hopane	1.06	1.05	0.67	0.55	0.56	0.64	0.58	0.7	0.64	0.61	0.59
$C_{29}Ts/(C_{29}Ts + C_{29}\alpha\beta$hopane)	0	0	0.12	0.15	0.24	0.14	0.18	0.18	0.09	0.11	0.12
$(C_{29}/C_{27})\alpha\alpha\alpha$-20R sterane	15.63	26.31	3.02	8.64	25.18	12.89	16.42	1.72	14.46	15.14	29.22
$(C_{29}/C_{28})\alpha\alpha\alpha$-20R sterane	2.76	2.71	2.61	2.7	2.8	2.71	2.8	1.87	4.11	2.96	3.27
$C_{29}\alpha\alpha\alpha$-20S/(20S + 20R)	0.45	0.45	0.44	0.46	0.47	0.47	0.48	0.42	0.47	0.49	0.49
$C_{29}\alpha\beta\beta/(\alpha\beta\beta + \alpha\alpha\alpha)$ sterane	0.27	0.25	0.43	0.47	0.48	0.47	0.49	0.57	0.47	0.49	0.49
$C_{27}\alpha\alpha\alpha$-20R sterane (%)	4.49	2.7	19.32	7.79	2.84	5.36	4.3	27.49	5.27	4.71	2.55
$C_{28}\alpha\alpha\alpha$-20R sterane (%)	25.4	26.21	22.33	24.9	25.6	25.54	25.16	25.24	18.53	24.05	22.85
$C_{29}\alpha\alpha\alpha$-20R sterane (%)	70.11	71.09	58.35	67.31	71.56	69.1	70.54	47.27	76.2	71.24	74.6
$8\beta(H)$-homodrimane/$8\beta(H)$-drimane	8.7	25.55	5.92	5.57	7.25	13.91	22.28	10.11	6.59	4.97	4.67
$8\beta(H)$-homodrimane/C_{30} hopane	0.1	0.03	0.13	0.69	0.78	0.29	0.24	1.22	0.21	0.21	0.32
$16\beta(H)$-phyllocladane/C_{30} hopane	2.45	1.39	0.17	10.34	1.59	0.84	0.69	11.19	0.79	1.2	0.72
dibenzothiophenes/phenanthrene (DBT/P)	0.04	0.04	0.08	0.13	0.12	0.13	0.08	0.08	0.08	0.08	0.08
R_{dit}	0.01	0.02	0.26	0.06	0.11	0.14	0.1	0.07	0.05	0.05	0.05

https://doi.org/10.1021/acsearthspacechem.2c00241
ACS Earth Space Chem. 2023, 7, 92−109

Table 1. continued

parameters	sample no.												
	ZBHC-5	ZBHC-1	ZBHC-2	ZBHC-3	ZBL-2	ZBL-6	ZBL-7	ZBL-9	ZBL-13	ZBL-15	ZBL-16	ZBL-18	ZBL-24
formation	C_1j	C_1j	C_1j	C_1j	C_1j	C_1j	C_1j	C_1j	C_1j	C_1j	C_1j	C_1j	C_1j
CPI_{22-32}[a]	1.23	1.2	0.82	1.19	1.22	1.13	1.12	1.09	1.08	1.11	1.05	1.03	0.78
TAR	0.31	0.39	0.18	0.08	0.36	0.17	0.14	0.11	0.12	0.12	0.06	0.02	
Pr/Ph	1.39	2.22	2.25	1.18	2.76	2.54	2.10	2.52	2.49	1.94	1.87	1.29	0.40
Pr/nC_{17}	0.6	0.74	0.59	0.84	0.82	0.61	0.65	0.66	0.57	0.59	0.42	0.41	0.42
Ph/nC_{18}	0.42	0.3	0.26	0.66	0.23	0.20	0.30	0.20	0.18	0.21	0.18	0.18	0.49
$\sum C_{21-}/\sum C_{22+}$	1.00	0.84	1.31	1.00	1.04	1.55	1.80	1.67	1.82	1.73	2.29	2.13	1.96
Ts/Tm	0.42	0.21	0.26	1.49	0.08	0.07	0.07	0.09	0.17	0.11	0.15	0.21	0.94
Ts/(Ts + Tm)	0.29	0.18	0.21	0.6	0.07	0.07	0.07	0.08	0.15	0.10	0.13	0.17	0.49
$C_{31}\alpha\beta$-22S/(22S + 22R)	0.58	0.58	0.58	0.56	0.59	0.59	0.58	0.59	0.57	0.58	0.58	0.58	0.51
$C_{32}\alpha\beta$-22S/(22S + 22R)	0.58	0.59	0.59	0.6	0.59	0.59	0.59	0.58	0.57	0.58	0.58	0.59	0.58
gammacerane index (GI)	0.06	0.06	0.05	0.15	0.07	0.05	0.05	0.06	0.08	0.09	0.07	0.08	0.23
C_{35}/C_{34} hopane	0.53	0.63	0.57	1	0.44	0.36	0.37	0.43	0.42	0.41	0.36	0.57	1.16
C_{19}/C_{23}TT	1	0.87	0.74	0.07	0.54	0.54	0.58	0.50	0.79	0.86	1.33	0.72	2.35
C_{20}/C_{23}TT	1.49	1.28	1.02	0.53	2.06	1.57	1.83	1.50	1.56	1.85	2.26	1.45	1.46
$(C_{19} + C_{20})$TT/C_{23}TT	2.5	2.14	1.76	0.6	2.60	2.11	2.41	2.00	2.35	2.71	3.59	2.17	3.81
C_{24}TeT/(C_{24}TeT + C_{23}TT)	0.6	0.61	0.59	0.35	0.82	0.71	0.75	0.72	0.67	0.69	0.67	0.64	0.12
ETR	0.25	1.41	1.39	1.08	1.97	2.52	2.24	2.18	1.79	1.86	1.78	1.55	1.88
C_{24}TeT/C_{26}TT > 1.0	1.96	2.96	2.31	1.9	11.02	14.73	12.87	7.87	7.76	7.15	6.64	4.87	0.46
C_{31}R/C_{30}	0.33	0.37	0.37	0.23	0.43	0.47	0.46	0.44	0.43	0.44	0.47	0.41	0.22
ΣTT/Σhopanes	0.09	0.08	0.09	0.56	0.04	0.05	0.05	0.05	0.10	0.07	0.09	0.13	1.86
C_{23}TT/C_{30} hopane	0.05	0.05	0.06	0.56	0.01	0.02	0.01	0.02	0.03	0.03	0.03	0.05	0.78
$C_{29}\alpha\beta/(\alpha\beta + \beta\alpha)$ hopane	0.83	0.84	0.86	0.87	0.88	0.91	0.91	0.90	0.90	0.90	0.89	0.86	0.90
$C_{30}\alpha\beta/(\alpha\beta + \beta\alpha)$ hopane	0.82	0.8	0.81	0.89	0.83	0.87	0.87	0.86	0.88	0.86	0.86	0.84	0.86
$C_{29}/C_{30}\alpha\beta$ hopane	0.71	0.81	0.8	0.58	0.67	0.52	0.51	0.52	0.47	0.48	0.50	0.52	0.56
C_{29}Ts/(C_{29}Ts + $C_{29}\alpha\beta$hopane)	0.22	0.15	0.15	0.24	0.07	0.06	0.06	0.06	0.10	0.08	0.09	0.13	0.23
$(C_{29}/C_{27})\alpha\alpha\alpha$-20R sterane	3.75	3.57	4.03	1.35	2.71	3.52	3.47	2.87	2.72	2.91	3.17	3.10	1.08
$(C_{29}/C_{28})\alpha\alpha\alpha$-20R sterane	4.34	4.94	3.81	1.45	4.97	4.47	4.97	4.43	3.72	3.99	4.48	3.53	1.16
$C_{29}\alpha\alpha\alpha$-20S/(20S + 20R)	0.45	0.45	0.47	0.47	0.47	0.46	0.45	0.46	0.46	0.46	0.46	0.47	0.44
$C_{29}\alpha\beta\beta/(\alpha\beta\beta + \alpha\alpha\alpha)$ sterane	0.37	0.37	0.39	0.4	0.43	0.47	0.47	0.46	0.48	0.46	0.47	0.47	0.41
$C_{27}\alpha\alpha\alpha$-20R sterane (%)	17.82	18.88	16.43	30.57	23.49	18.84	19.34	22.12	22.44	21.59	20.52	20.08	33.24
$C_{28}\alpha\alpha\alpha$-20R sterane (%)	15.39	13.66	17.38	28.29	12.81	14.83	13.51	14.34	16.42	15.71	14.50	17.66	30.92
$C_{29}\alpha\alpha\alpha$-20R sterane (%)	66.8	67.46	66.2	41.15	63.70	66.33	67.15	63.54	61.14	62.71	64.98	62.27	35.84
$8\beta(H)$-homodrimane/$8\beta(H)$-drimane	3.53	3.15	3.88	2.54	9.30	6.32	5.50	10.76	12.82	9.90	8.93	10.98	
$8\beta(H)$-homodrimane/C_{30} hopane	0.31	0.21	0.16	0.12	0.05	0.07	0.04	0.10	0.03	0.08	0.02	0.03	
$16\beta(H)$-phyllocladane/C_{30} hopane	0.03	0.02	0.02	0.11	0.00	0.01	0.00	0.08	0.01	0.11	0.03		0.29
dibenzothiophenes/phenanthrene (DBT/P)	0.06	0.06	0.06	0.1	0.05	0.06	0.05	0.06	0.06	0.06	0.06	0.05	0.04
R_{dit}	2.42	0.82	0.97	1.49	1.51	1.35	1.40	1.80	2.67	2.63	2.45	1.49	6.90

[a] $CPI_{22-32} = 2 \times (nC_{23} + nC_{25} + nC_{27} + nC_{29} + nC_{31})/(nC_{22} + 2 \times nC_{24} + 2 \times nC_{26} + 2 \times nC_{28} + 2 \times nC_{30} + nC_{32})$. TAR = $(nC_{27} + nC_{29} + nC_{31})/(nC_{15} + nC_{17} + nC_{19})$. ETR = $(C_{28} + C_{29})$ TT/Ts. R_{dit} = (19-norisopimarane + isopimarane + 16α-kaurane)/(ent-beyerane + 16β-phyllocladane + 16α-phyllocladane). Gammacerane index (GI) = gammacerane/C_{30} hopane.

https://doi.org/10.1021/acsearthspacechem.2c00241
ACS Earth Space Chem. 2023, 7, 92−109

compared with the mudstones (0.28−8.95 wt %, with an average value of 2.4 wt %).

S_1 and S_2 values of the studied samples were in the range of 0.06−5.51 mg HC/g rock and 0.25−46.54 mg HC/g rock, respectively. The S_1 and S_2 values of carbonaceous mudstones and tuffaceous mudstones (0.06−5.51 mg HC/g rock and 0.27−46.54 mg HC/g rock, respectively) are higher than that of mudstones (0.07−1.85 mg HC/g rock and 0.25−12 mg HC/g rock, respectively). T_{max} of the study samples falls in the range of 434−482 °C. The hydrogen index (HI) is an indicator for hydrocarbon generation potential and organic type, which ranges from 18.26 to 338 mg HC/g TOC (avg. = 104 mg HC/g TOC).

Because carbonaceous mudstones were more common in the Batamayineishan Formation, and the average values of TOC, S_1, S_2, and HI are higher for samples in the Batamyineishan Formation than those for samples in the Jiangbasitao Formation. T_{max} values and Ro of the samples in the Batamayineishan Formation are low.

4.3. Organic Petrology Characterization. Vitrinite is the dominant maceral group in the studied samples, followed by inertinite and liptinite. Vitrinite particles were present as hydrocarbon-rich vitrinite, collinite, telinite, and vitrodetrinite (Figures 4 and 5b). The shape of the vitrinite is banded. Most of the vitrinite has no fluorescence, while weak fluorescence could be observed in hydrocarbon-rich vitrinite. Inertinite was present mainly as micrinite (M) (Figure 5a). Trace amounts of liptinite particles are observed, including alginite (A) [telalginite (T) and lamalginite (L)], resinite (Re), fluorinate (Fl), and cutinite (Cu) (Figure 5). Lamalginite mainly shows the thin and long lamellae shape with yellow fluorescence. In addition, framboid pyrites were also observed in well ZBH, occurring as assemblages of recrystallized framboids (Figure 4). The Ro of studied samples ranges from 0.63 to 1.04%.

4.4. EOM and Carbon Isotope Compositions. The EOM contents and stable carbon isotope compositions are shown in Table S2 in the Supporting Information. EOM contents of carbonaceous mudstone samples are relatively higher (spanning from 2560 to 4002 ppm) than those of tuffaceous mudstone samples (556−2811 ppm, avg. = 1043 ppm) and mudstones (603−1297 ppm, avg. = 842 ppm). The percentage of hydrocarbon compounds (including saturates and aromatics) varies significantly, from 5 to 50% and 5 to 33%, respectively. The percentage of polar compounds (a sum of resin and asphaltene) is relatively higher than that of hydrocarbon compounds, ranging from 34 to 82%.

The $\delta^{13}C$ values of EOM, saturated fraction, and aromatic fraction fall in the range of −26.5−−23.0‰, −29.4−−25.7‰, and −27.7−−23.0‰, respectively. The $\delta^{13}C$ values of the resin fraction and asphaltene fraction range from −26.4 to −23.6‰ and from −26.0 to −22.6‰, respectively. The CV values (proposed by Sofer[18] to identify the OM inputs) are calculated using the equation below

$$CV = -2.53 \times \delta^{13}C_{saturates} + 2.22 \times \delta^{13}C_{aromatics} - 11.65$$

The CV values are spanning from −1.1 to 6.8, most of which are higher than 0.47, except those for sample ZBB-539 and sample ZBC-547.

4.5. Molecular Composition. *4.5.1. n-Alkanes and Acyclic Isoprenoids.* The distribution of *n*-alkanes, extending from C_{12} to C_{37}, is similar in the studied samples showing a unimodal pattern (Figure 5). The distribution patterns of *n*-alkane are dominated by low-molecular-weight *n*-alkanes (*n*-C_{15}-*n*-C_{19}) and medium-molecular-weight *n*-alkanes (*n*-C_{20}-*n*-C_{26}) with a medium to high $\sum C_{21-}/\sum C_{22+}$ ratio, ranging from 0.65 to 2.44 (Figure 5 and Table 1). The carbon preference index (CPI_{22-32}) falls between 0.78 and 1.34 (avg. = 1.07). The TAR is defined as $(nC_{27} + nC_{29} + nC_{31})/(nC_{15} + nC_{17} + nC_{19})$. It is related to the terrestrial/aquatic sources of sediments,[19] falling between 0.02 and 0.45. Acyclic isoprenoids are detected in all samples in significant amounts with pristane/phytane (Pr/Ph) ratios of most samples being in the range of 1−2. Pr/Ph values for samples from the Upper Batamayineishan Formation were high (4.44 for sample ZBCC-40 and 4.09 for sample ZBCC-21), while those were low for samples from the Lower Jiangbasitao Formation (0.63 for ZBL-23 and 0.40 for ZBL-24). The Pr/nC_{17} and Ph/nC_{18} ratios range from 0.41 to 1.95 and 0.13 to 0.66, respectively (Table 1).

4.5.2. Sesquiterpenoids and Diterpenoids. Aliphatic sesquiterpenoids were observed in the studied samples, including C_{14}, C_{15}, and C_{16} bicyclic sesquiterpenoids. 8$\beta(H)$-drimane and 8$\beta(H)$-homodrimane were detected in all samples. 8$\beta(H)$-homodrimane/8$\beta(H)$-drimane and 8$\beta(H)$-homodrimane/C_{30} hopane ratios span from 2.54 to 25.55 and from 0.03 to 1.22, respectively. A series of aliphatic and aromatic diterpenoids were detected in the Carboniferous source rocks, including ent-beyerane, isopimarane, 16$\beta(H)$-phyllocladane, abietane, ent-16$\beta(H)$-kaurane, 16$\alpha(H)$-phyllocladane, and retene. 16$\beta(H)$-phyllocladane and ent-16$\beta(H)$-kaurane are present in all C_2b samples. The 16$\beta(H)$-phyllocladane/C_{30} hopane ratio ranges from 0 to 11.19. Diterpenoids (such as 16$\beta(H)$-phyllocladane) are predominant sesquiterpenoids in the C_2b samples and several C_1j samples (the upper part of the Jiangbasitao Formation in well ZBB). The 16$\beta(H)$-phyllocladane/C_{30} hopane ratio for the C_2b samples is much higher than that of the C_1j samples in the wells ZBH and ZBL (Table 1). Retene is the dominant compound among the aromatic diterpenoids in all samples.

4.3.3. Tricyclic Terpanes and Pentacyclic Triterpenoids. The series of C_{19} to C_{29} tricyclic terpanes (TTs) and C_{24} tetracyclic terpane (TeT) were detected in the Carboniferous sediments. C_{24} TeT contents are very high, presenting as the dominant compound in most samples. ΣTT/Σhopanes and $C_{23}TT/C_{30}$ hopane ratios are in the range of 0.02−1.82 and 0.004−0.78, respectively. $C_{24}TeT/(C_{24}TeT + C_{23}TT)$, $C_{24}TeT/C_{26}TT$, and ETR (ETR = $(C_{28} + C_{29})TT/Ts$) values range from 0.12 to 0.88, from 0.46 to 14.73, and from 0.25 to 2.69, respectively. In contrast, $(C_{19} + C_{20})TT/C_{23}TT$ values for most C_1j samples (avg. = 2.78) are lower than that of C_2b samples (avg. = 6.06).

Abundant pentacyclic triterpenoids were detected in all studied samples, including C_{27} to C_{35} hopane, which were dominated by 17$\alpha(H)$,21$\beta(H)$−C_{30} hopane ($C_{30}\alpha\beta$H) or 17$\alpha(H)$,21$\beta(H)$−C_{29} hopane ($C_{29}\alpha\beta$H). C_{27} hopanes, including 18$\alpha(H)$-22,29,30-trisnorneohopane (Ts) and 17$\alpha(H)$-22,29,30-trisnorhopane (Tm), were present in all samples. Ts/(Ts + Tm) ratios range from 0.03 to 0.93. Both $C_{31}\alpha\beta$-22S/(22S + 22R) homohopanes and $C_{32}\alpha\beta$-22S/(22S + 22R) homohopanes ratios are high. They are in the range of 0.51−0.59 and 0.56−0.60, respectively. Both of them have reached equilibrium. $C_{29}\alpha\beta/(\alpha\beta + \beta\alpha)$ hopane and $C_{30}\alpha\beta/(\alpha\beta + \beta\alpha)$ hopane ratios are in the range of 0.77−0.91 and 0.68−0.93, respectively. $C_{29}Ts/(C_{29}Ts + C_{29}\ \alpha\beta$ hopane), C_{35}/C_{34} hopane ratios and gammacerane index (gammacerane/$C_{30}\ \alpha\beta$ hopane) span from 0 to 0.24, 0.36 to 1.21, and 0 to 0.3, respectively.

https://doi.org/10.1021/acsearthspacechem.2c00241
ACS Earth Space Chem. 2023, 7, 92−109

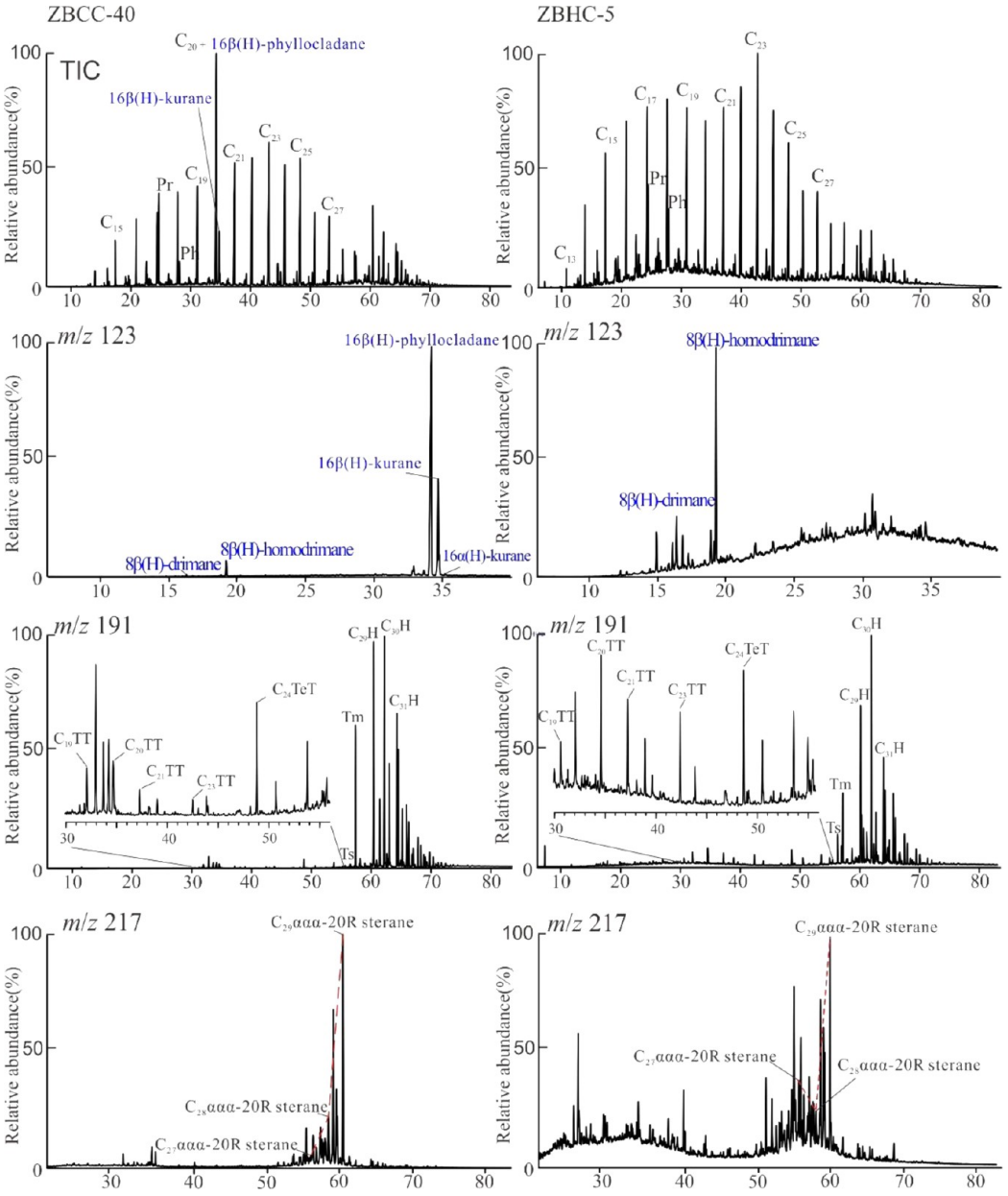

Figure 6. TIC and partial mass chromatograms (m/z 191, m/z 217, and m/z 123) of the aliphatic hydrocarbons in two representative samples, exhibiting the relative abundance of *n*-alkanes, TTs, TeTs, hopenes, steranes, sesquiterpenoids, and diterpenoids.

4.3.4. Steranes. Steranes were also analyzed in this study. For the samples from the Batamayinieshan Formation (in well ZBC) and the samples from the Upper Jiangbasitao Formation (in well ZBB), steranes were dominated by the $C_{29}\alpha\alpha\alpha$-20R sterane indicated by the strongest peak in the studied samples, followed by $C_{28}\alpha\alpha\alpha$-20R sterane and $C_{27}\alpha\alpha\alpha$-20R sterane. The relative abundance of $C_{27}\alpha\alpha\alpha$-20R is higher than that of $C_{28}\alpha\alpha\alpha$-20R sterane for the C_1j samples (in wells ZBH and ZBL) (Table 1). C_{29}/C_{27} $\alpha\alpha\alpha$-20R sterane and C_{29}/C_{28} $\alpha\alpha\alpha$-20R sterane ratios are ranging from 1.08 to 29.22 and from 1.16 to 4.97, respectively. The relatively less stable $C_{29}\alpha\alpha\alpha$-20R sterane and $C_{29}\alpha\alpha\alpha$ sterane are more abundant compared to the $C_{29}\alpha\alpha\alpha$-20S sterane and $C_{29}\alpha\beta\beta$ sterane, with the $C_{29}\alpha\alpha\alpha$-20S/(20S + 20R) and $C_{29}\alpha\beta\beta/(\alpha\beta\beta + \alpha\alpha\alpha)$ sterane ratios varying from 0.42 to 0.49 and 0.25 to 0.57, respectively.

5. DISCUSSION

5.1. Organic Matter Abundance and Genetic Type. TOC, S_1, and S_2 are the most basic and commonly used indicators for the assessment of hydrocarbon generation potential. As mentioned above, carbonaceous mudstones and tuffaceous mudstones have higher TOC, S_1, and S_2 content than mudstones. Particularly, it can be concluded from the plots of S_2 versus TOC that most samples have fair to excellent source rock richness (Figure 7). The production yield (PY, S_1 + S_2) falling between 0.32 and 49.24 mg HC/g rock with an average of 9.14 mg HC/g rock also suggests a generally good petroleum or gas latent capacity. The wide range of PY is mainly controlled by the OM abundance.

Pyrolysis data were widely applied to evaluate the genetic type of OM.[20−23] Most of the studied samples are gas-prone, which is indicated by the low HI (less than 300 mg HC/g TOC). As shown in Figures 7 and 8, most samples were plotted in the zone

https://doi.org/10.1021/acsearthspacechem.2c00241
ACS Earth Space Chem. 2023, 7, 92−109

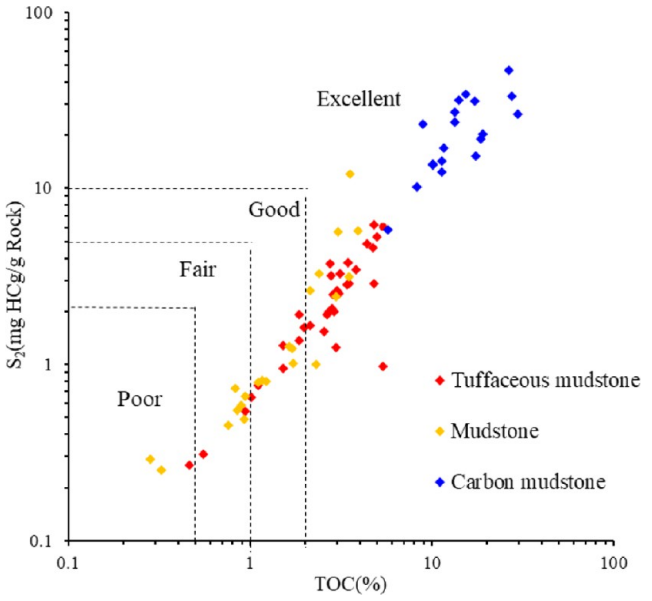

Figure 7. Cross-plots of S_2 vs TOC for study samples.

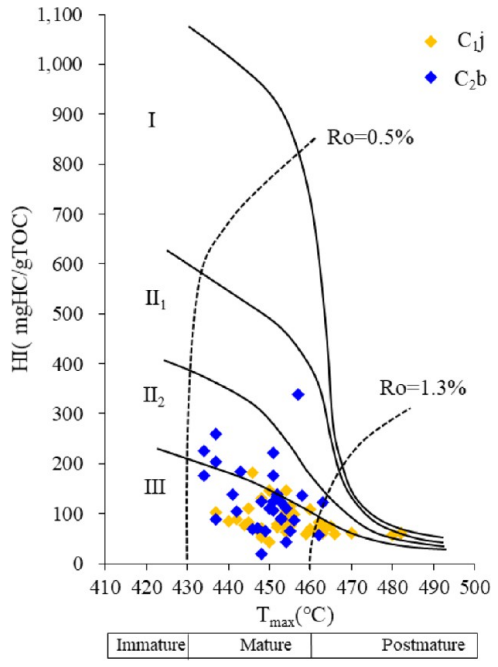

Figure 8. Diagram of HI vs T_{max} of the study source rocks.

of type III kerogen with a little portion plotted in the zone of type II_2 kerogen. 30% of the source rocks in the Batamayineishan Formation were plotted in the zone of type II_2–II_1 kerogen, while most of the source rocks in the Jiangbasitao Formation were plotted in the zone of type III kerogen except the sample ZBL-23 and the sample ZBL-24. It can be also supported by the presence of large amounts of vitrinite maceral. Additionally, the presence of resinite, alginate (telalginite and lamalginite), resinite, cutinite, and hydrocarbon-rich vitrinite may indicate some petroleum generation potential of the Carboniferous sediments.

5.2. Thermal Maturity of OM. Maceral compositions of the studied samples were dominated by vitrinite, and the vitrinite reflectance can be used to evaluate the thermal maturity of samples. Random vitrinite reflectance (Rr) of the studied samples falls between 0.63 and 1.04%, suggesting a primarily mature stage. As shown in Figure 9, the study samples were

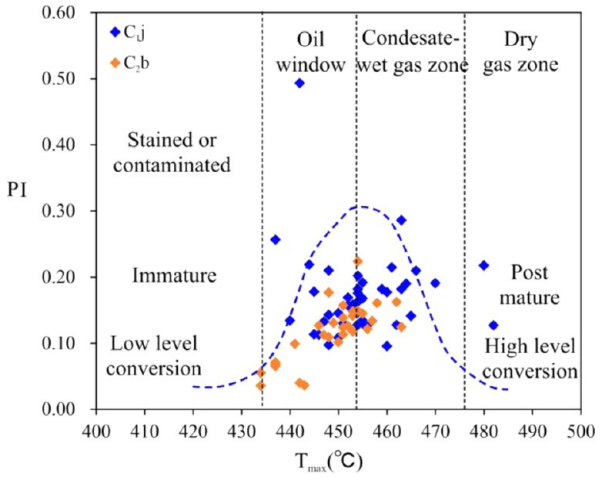

Figure 9. Diagram of T_{max} vs PI of study samples from the Shibei Sag, Junggar Basin. Genetic lines are from Peters and Cassa.[20]

mainly plotted in the oil window and condensate-wet gas zone, suggesting its good hydrocarbon generation conditions. In addition, the biomarker parameters are also useful to evaluate maturity. The C_{31} 22S/(22S + 22R) homohopane ratio and C_{32} 22S/(22S + 22R) homohopane ratio have achieved equilibrium (0.57–0.62),[19,24] indicating that all study samples were in or exceeded the early maturation stage (Table 1). C_{29} $\alpha\beta/(\alpha\beta + \beta\alpha)$ hopane and C_{30} $\alpha\beta/(\alpha\beta + \beta\alpha)$ hopane ratios can be used for slightly higher maturity source rocks, while C_{31}22S/(22S + 22R) and C_{32} 22S/(22S + 22R) homohopane ratios are used for relatively lower maturity source rocks. Their equilibrium value is around 0.9, which can reflect an early oil generation stage. As shown in Figure 10, both $C_{29}\alpha\alpha\alpha$20S/(20S + 20R) versus $C_{29}\alpha\beta\beta/(\alpha\beta\beta + \alpha\alpha\alpha)$ sterane[18] cross-plots and C_{29} $\alpha\beta/(\alpha\beta + \beta\alpha)$ hopane versus C_{30} $\alpha\beta/(\alpha\beta + \beta\alpha)$ hopane[25] cross-plots suggest that the Carboniferous source rocks were mature. Besides, low tricyclic/17α hopane values also suggest a medium maturity (Table 1).

However, from the seismic section (Figure 3), we can find that three boreholes in our study did not reach the bottom of the Jiangbasitao Formation, and there are very thick strata below. High Ro of the lower strata together with the occurrence of the condensate in well ZBH suggests a good condensate-wet gas generation potential.

5.3. Origins and Depositional Conditions of Organic Matter. The kerogen carbon isotope ($\delta^{13}C_{kerogen}$) composition is generally considered as an effective proxy to identify the OM type, especially for highly mature or overmature hydrocarbon source rocks.[26] It is reported that $\delta^{13}C_{kerogen}$ values > −26‰ indicate the humic (type III) kerogen type, while $\delta^{13}C_{kerogen}$ values < −28‰ indicate the sapropelic (type I) kerogen type. Also, $\delta^{13}C_{kerogen}$ values ranging from −28 to −26‰ suggest a mixed kerogen type (type II).[26] The $\delta^{13}C_{kerogen}$ of most studied samples was greater than −26‰ except the samples ZBC-549 and ZBC-547, suggesting a predominant contribution of terrigenous OM, which is also supported by the cross-plots of $\delta^{13}C_{saturates}$ versus $\delta^{13}C_{aromatics}$ (Figure 11). The OM with CV (CV = −2.53 × $\delta^{13}C_{sat}$(‰) + 2.22 × $\delta^{13}C_{aro}$ (‰) −11.65) > 0.47 is generally thought to be derived from higher plant inputs, while CV < 0.47 is related to planktons.[18] The higher CV values

https://doi.org/10.1021/acsearthspacechem.2c00241
ACS Earth Space Chem. 2023, 7, 92–109

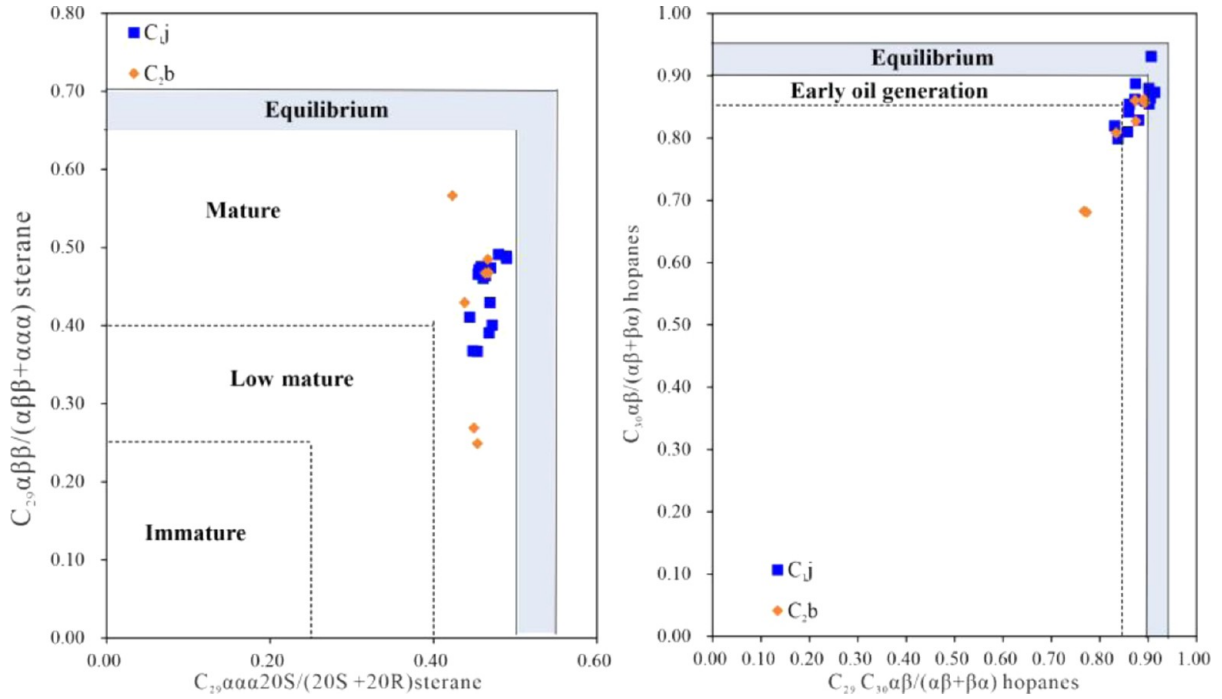

Figure 10. Plots of (a) $C_{29}\alpha\alpha\alpha 20S/(20S + 20R)$ vs $C_{29}\alpha\beta\beta/(\alpha\beta\beta + \alpha\alpha\alpha)$ sterane[18] and (b) C_{29} $C_{30}\alpha\beta/(\alpha\beta + \beta\alpha)$ hopanes vs $C_{30}\alpha\beta/(\alpha\beta + \beta\alpha)$ hopanes[25] in the Carboniferous sediments from the Shibei Sag, Junggar Basin.

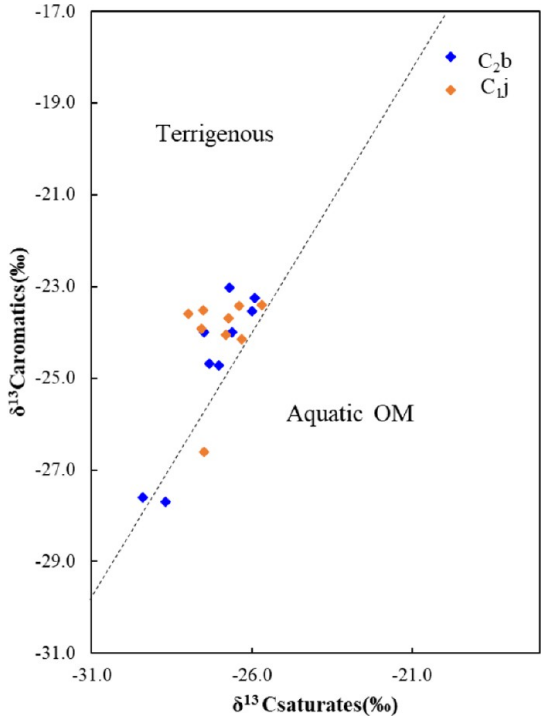

Figure 11. Cross-plots of $\delta^{13}C_{saturates}$ vs $\delta^{13}C_{aromatics}$ of study samples from the Shibei Sag, Junggar Basin.

of the studied samples suggest the predominant higher plant inputs with a minor contribution of planktons. This is consistent with the results of organic petrological observations. It was demonstrated that most lamalginites were derived from the planktonic algae (such as Pediastrum) or were similar enough to the recognizable planktonic material when a planktonic origin is possible.[18] Resinite (Re), fluorinite (Fl), and cutinite (Cu) mainly originate from cell excretions, leaves, and stems in gymnosperms or angiosperms.[27] The predominant macerals of vitrinite and inertinite with some liptinite in the studied sample also suggest the dominant contribution of higher plants.

The biomarker characteristic is a common and effective indicator for OM origin assessment.[20,28−30] Cross-plots of Pr/nC$_{17}$ versus Pr/nC$_{18}$ show that the Carboniferous sediments are characterized by terrestrial and mixed OM, and they are mainly deposited in a sub-oxic to oxic environment (Figure 12). The

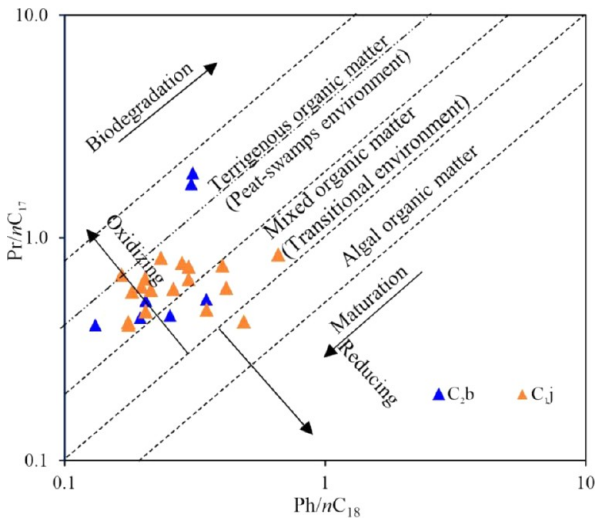

Figure 12. Diagram of Pr/nC$_{17}$ vs Pr/nC$_{18}$ of the study samples.

medium values of $\sum C_{21-}/\sum C_{22+}$ suggested the contribution of terrestrial and/or algal inputs, and this could be attributed to the pre-terrestrial plants which lacked long-chain n-alkanes and had not evolved into "real" higher plants in early Carboniferous.[31] It is similar to the Carboniferous sediments in the Ruhr Basin, western Germany, which exhibited a predominance of medium-

https://doi.org/10.1021/acsearthspacechem.2c00241
ACS Earth Space Chem. 2023, 7, 92−109

molecular-weight *n*-alkanes.[26] Notably, the samples from the Upper Batamayineishan Formation (ZBC-40 and ZBC-21) were plotted in the peat-swamp environment zone, and the samples from the Lower Jiangbasitao Formation (ZBL-24) were plotted in a reducing environment zone (Figure 12). There seems to be a transition of the environment from reducing to oxidizing with terrigenous OM inputs.

C_{19} and C_{20} TTs are generally thought to be related to terrigenous higher plants[20] (e.g., vascular plants), while C_{23} TTs are mainly predominant in reduced marine sediments with aquatic OM.[49−51] High C_{19}/C_{23}TT and C_{20}/C_{23}TT ratios of the C_2b samples suggest a high contribution from terrigenous OM. This is consistent with the fact that ETR < 2 and C_{24}TeT/C_{26}TT > 1.0 in most study samples, which suggests that the source rocks were deposited under mainly freshwater, suboxic to dysoxic conditions with considerable terrestrial inputs.[52] The ratios of C_{24} TeT/(C_{24} TeT + C_{23} TT) are higher than 0.5 in the studied samples, indicating the significant contribution of terrigenous OM. C_{35}/C_{34} 22S homohopanes < 0.6 indicate the contribution of terrestrial resins.[20] Low ratios of C_{35}/C_{34} (avg. = 0.54) are indicative of terrigenous OM inputs under oxic conditions. C_{27} and C_{28} regular steranes were commonly thought to be linked to planktons/phytoplanktons, while C_{29} regular steranes were derived from terrigenous OM.[53] There were also research studies showing that C_{29} regular steranes can be derived from green and brown algae besides terrigenous OM.[54−56] The ternary diagram of the proportion of C_{27}−C_{28}−C_{29} $\alpha\alpha\alpha$-20R steranes (Figure 13) shows the predominant contribution of

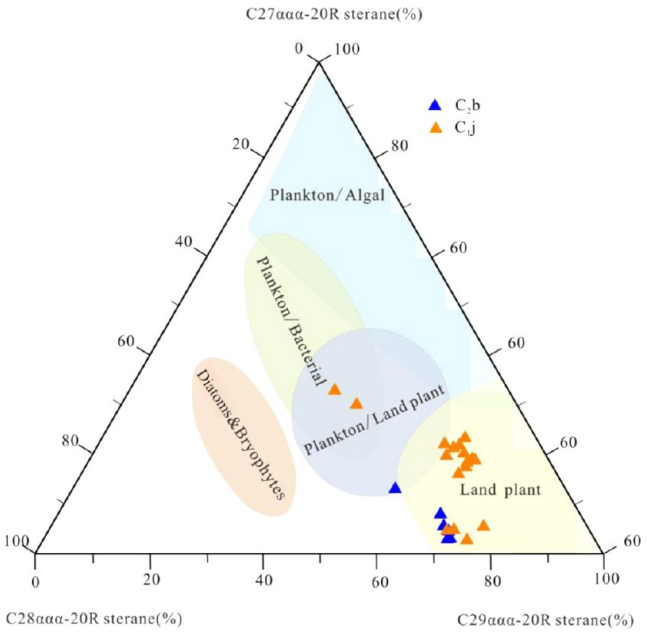

Figure 13. Ternary diagram of $C_{27}\alpha\alpha\alpha$ (20R), $C_{28}\alpha\alpha\alpha$ (20R), and $C_{29}\alpha\alpha\alpha$ (20R) steranes of the Carboniferous source rocks from the Shibei Sag, Junggar Basin.

land plants, but we cannot rule out the minor contribution of algae which can be supported by the presence of alginite, telalginite, and lamalginite. In addition, it can be found that the C_1j samples (in the well ZBH and the well ZBL) and the C_2b samples (in the well ZBC) were plotted in different areas (Figure 13), indicating their different origins.

Bicyclic sesquiterpenoids are widely thought to be related to resins of higher plants,[32−35] although they are also probably derived from prokaryotic bacteria.[34,36,37] There were many diterpenoids detected in source rocks, coal, and fossil resins.[38−46] They were generally regarded as indicators of conifer plants. Phyllocladanes are the typical indicator for gymnosperms or pre-gymnosperms. They were first identified and applied in the research of the Pennsylvanian sediments in the Ruhr and Saar basins.[47] Abundant bicyclic sesquiterpenoids and diterpenoid biomarkers detected in the studied samples suggest the conifer inputs in the Carboniferous sediments (e.g., the Voltziales[47]). However, compared with the C_2b samples, only minor amounts of diterpenoid biomarkers were detected in the C_1j samples (in wells ZBH and ZBL) (Figure 6). This indicates that scarce higher plants grew in the ZBL and ZBH areas during the early Carboniferous period. Only trace pimaranes were detected. Accordingly, aromatic diterpenoids such as simonellite are absent. The high amount of phyllocladanes and retene and shortage of simonellite indicate the presence of conifer species of families other than Pinaceae.[44] Fleck[48] had applied the diterpane ratio R_{dit} as (19-norisopimarane + isopimarane + 16α-kaurane)/(ent-beyerane + 16β-phyllocladane + 16α-phyllocladane) to determine the contributions of pteridophytes and pre-gymnosperms. R_{dit} >1.5 suggests that pteridophytes predominate pre-gymnosperms, and this can be linked to swamp conditions, while R_{dit} <1.1 suggests the vice versa. The R_{dit} ratios of most C_1j samples (in wells ZBH and ZBL) are higher than 1.5, indicating that pteridophytes predominate pre-gymnosperms during the early Carboniferous period, and the climate was wet with a high water table. In contrast, the R_{dit} ratios of all C_2b samples and C_1j samples of the well ZBB are lower than 1.1, indicating that pre-gymnosperms predominate pteridophytes during the late Carboniferous period (Table 1). The climate was probably dry during this period which was likely linked to a low water table in the swamps. Kauranes are detected in the studied samples except samples in the well ZBH, suggesting the existence of gymnosperms, pre-gymnosperms, pteridophytes, or bryophytes in swamps.[30]

The sedimentary environment of the study area is very complex during the Carboniferous period. As mentioned in Section 4.1, the Carboniferous source rocks were mainly deposited with tuff layers during the interval of the volcano eruptions. Previous studies have proved that volcanic ash plays an important role in the accumulation of OM.[57−60] Thus, abundant ash can take nutrients to the water. Generally, Pr/Ph > 3.0 indicates an oxic depositional environment, while Pr/Ph < 1.0 represents a reducing depositional environment.[20] The Pr/Ph values of the Carboniferous sediments suggest an oxic to suboxic depositional condition. In particular, Pr/Ph values of samples in the Upper Batamayineishan Formation (samples ZBCC-40 and ZBCC-21) are higher than 4, suggesting a more oxic environment in the late Carboniferous. However, low Pr/Ph values for samples of the Lower Jiangbasitao Formation suggest a reducing environment, which can be also confirmed by the plot of Pr/nC_{17} versus Ph/nC_{18} (Figure 12). All studied samples were plotted into the peat/swamp zone and the transitional zone. Only a low amount of gammacerance and no β-carotane were detected in most analyzed samples (except sample ZBL-24), suggesting a freshwater condition.

The high concentrations of DBT and MDBT are generally indicative of marine shale or carbonates, whereas their low concentrations suggest an oxic continental environment.[61] Low DBT/P ratios indicate low organic sulfur contents in the analyzed samples. The presence of framboidal pyrites with larger

https://doi.org/10.1021/acsearthspacechem.2c00241
ACS Earth Space Chem. 2023, 7, 92−109

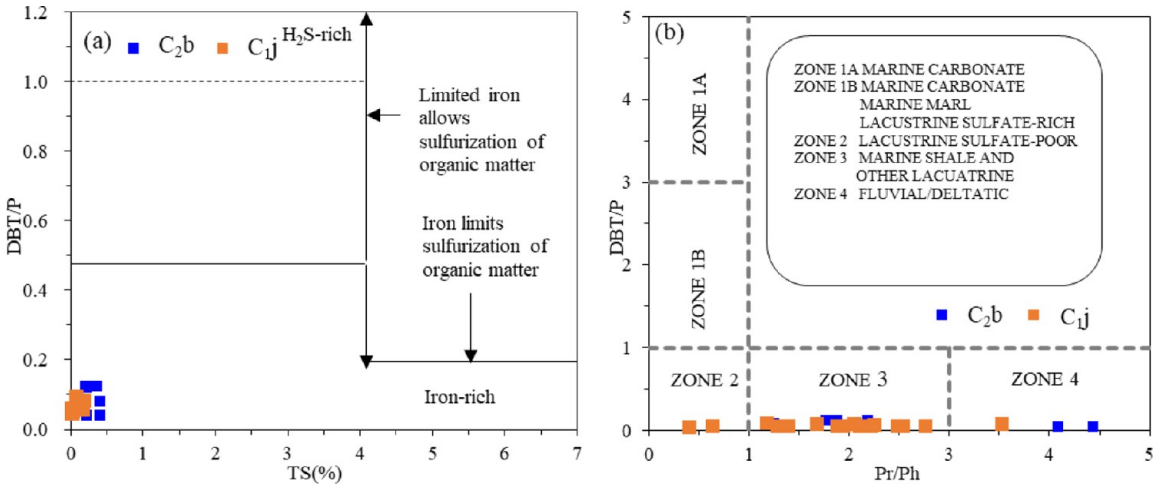

Figure 14. Dibenzothiophene/phenanthrene ratio vs TS values (a) and Pr/Ph (b) reflecting depositional environment of the Carboniferous source rocks from the Shibei Sag, Junggar Basin.

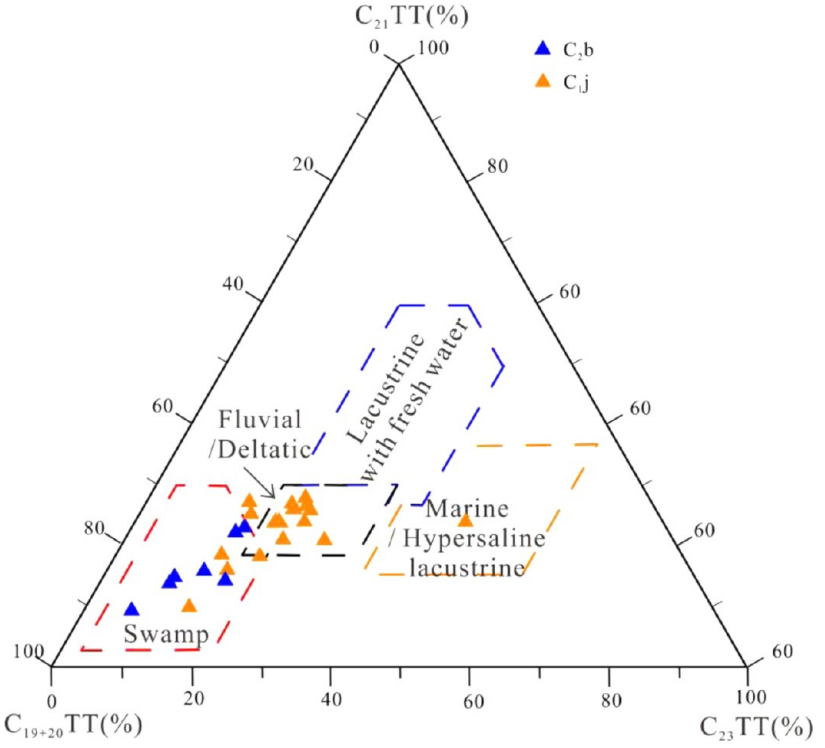

Figure 15. Ternary plot of C_{21}TT, C_{23}TT, and C_{19+20}TT showing the depositional environments for the studied samples.

diameters is an inorganic proxy of oxic depositional conditions.[62] Low organic sulfur contents of the Carboniferous source rocks can be explained by the low sulfurization of OM which is limited by the sufficient iron[63] (Figure 14a). The occurrence of iron leads to the formation of pyrite using the sulfur, and this is typical in sulfate-lacked freshwater.[64−66] Additionally, in the cross-plots of DBT/P versus Pr/Ph, most studied samples were plotted into the "marine shale and other lacustrine" field, and two carbonaceous mudstone samples of the Upper Batamayineishan Formation correspond to the "fluvial/deltaic" area (Figure 14b). In addition, the C_{31} 22R/C_{30} hopane ratio is generally low (<0.25) for lacustrine deposits and high for marine deposits.[20,67] Sediments deposited in lacustrine environments usually have a low $C_{29}/C_{30}\alpha\beta$ hopane ratio (<0.7).[20,67] However, in our samples, slightly high C_{31} 22R homohopane/C_{30} hopane ratios (avg. = 0.35) and $C_{29}/C_{30}\alpha\beta$ hopane ratio (avg. = 0.7) may indicate a transitional environment. The distribution of TTs is an indicator of the depositional environment, and Xiao et al.[68] proposed an effective plate to discriminate source rocks and crude oils from various depositional environments. The studied samples of the Jiangbasitao Formation in the well ZBL and the well ZBH were plotted into the "Fluvial/Deltatic" field (except sample ZBHC-3). The C_2b samples of well ZBC and the C_1j samples of well ZBB were plotted into the "Swamp" zone (Figure 15). It can be concluded that the Carboniferous source rocks were deposited in a fluvial-deltaic environment with the oscillations of the water table.

In conclusion, the Carboniferous source rocks were mainly deposited in a transitional environment under lacustrine-fluvial/

https://doi.org/10.1021/acsearthspacechem.2c00241
ACS Earth Space Chem. 2023, 7, 92−109

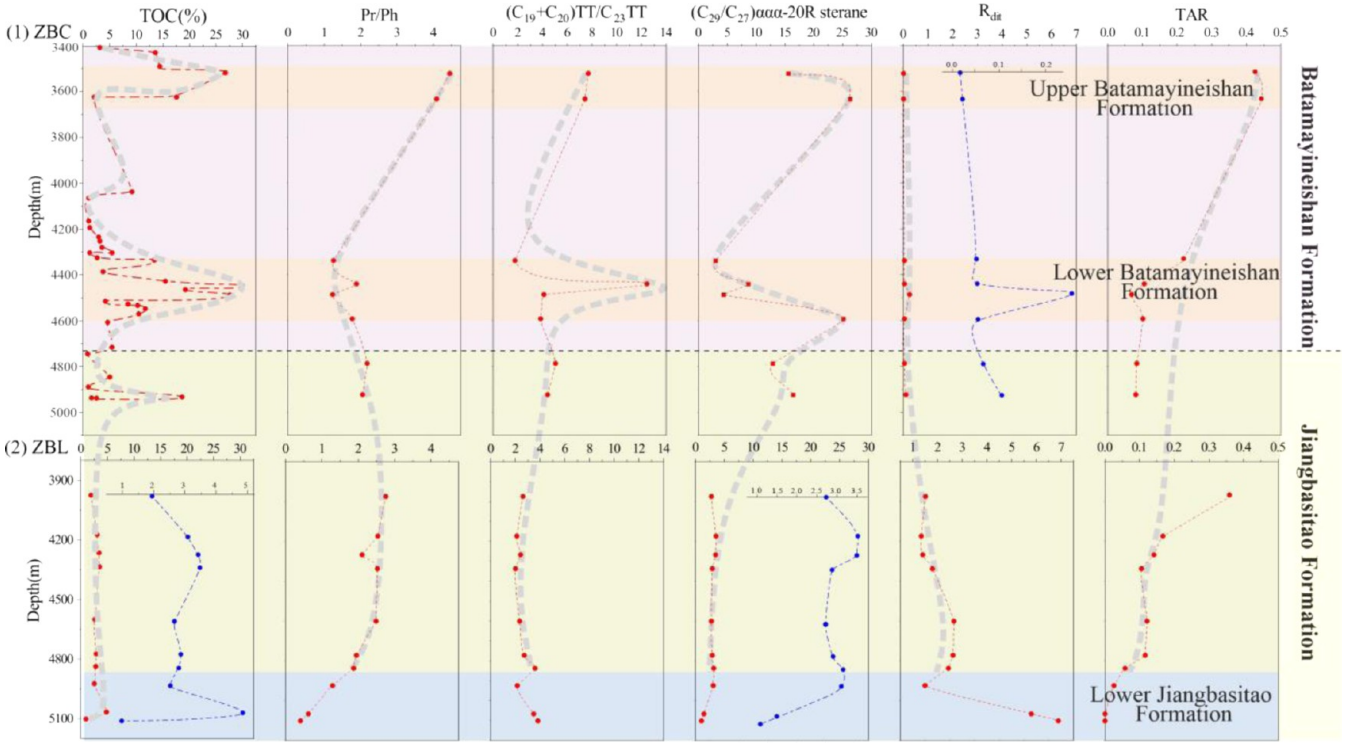

Figure 16. Profiles of the geochemical indices of the Carboniferous (the Jiangbasitao Formation and the Batamayineishan Formation) from (1) well ZBC and (2) well ZBL in the Shibei Sag, Junggar Basin.

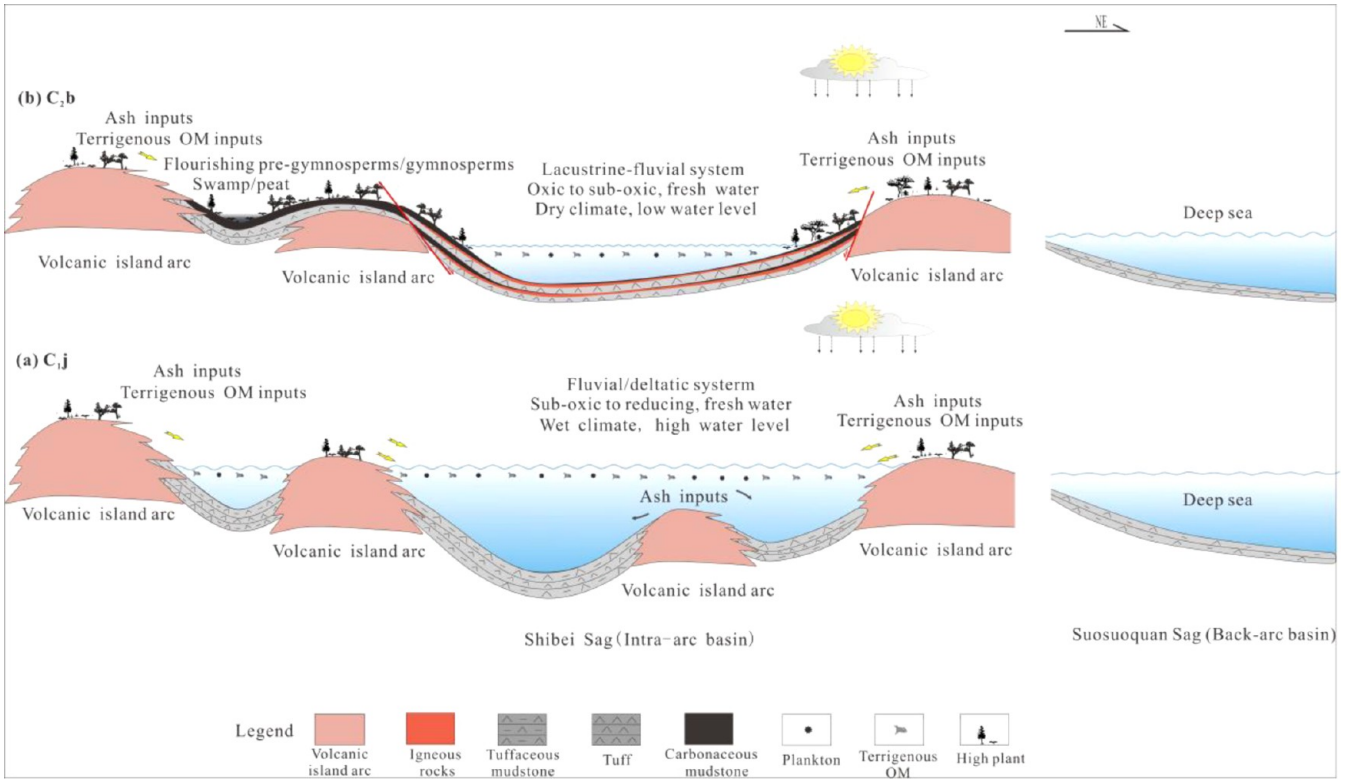

Figure 17. Schematic diagram of the OM input and the environment in the study area during the Carboniferous period.

deltaic conditions, particularly in a peat and swamp environment in ZBB and ZBC areas during the interval of the volcano eruption. The geochemical analysis results are also consistent with the common concept that peat or swamp facies with oxic conditions in prodelta is favorable to the deposition of coal-source rocks.

5.4. Sedimentary Model. Volcanic activities were active during the period of the Carboniferous. In the Carboniferous, the Shibei Sag is an intra-arc basin, and the source rocks were

https://doi.org/10.1021/acsearthspacechem.2c00241
ACS Earth Space Chem. 2023, 7, 92−109

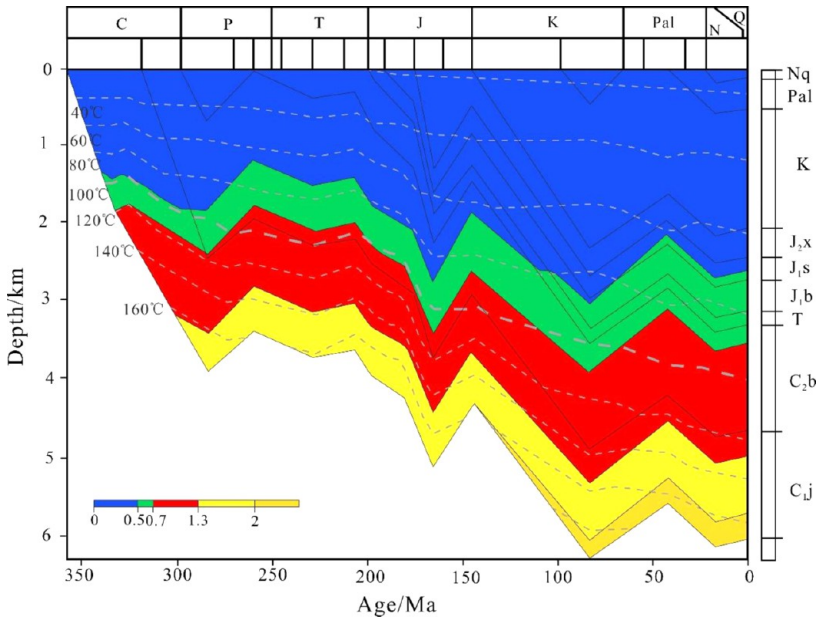

Figure 18. Diagram of the burial thermal evolution from the study area.

deposited during the interval of the volcanic eruptions. The cross-plots of Pr/nC$_{17}$ versus Ph/nC$_{18}$ indicate a complex transitional environment during the deposition of the Carboniferous source rocks. In the early Carboniferous (C$_1$j), type III source rocks were deposited in a sub-oxic to reducing environment. High R_{dit} values indicate a wet climate with a high water level which can be induced by the water pouring from the Suosuoquan Sag. In contrast, the depositional environment for the late Carboniferous (C$_2$b) is more oxic. The high relative abundance of diterpenoid and C$_{29}$ $\alpha\alpha\alpha$-20R sterane biomarkers suggests the flourishing of in situ higher plants (pre-gymnosperms) under a dry condition with a low water level in this period (Figure 16). Active volcanic eruptions bring large amounts of ash into the lake or delta, which allows higher plants to expand rapidly. Therefore, in the restricted bay, gymnosperms/pre-gymnosperms flourished in the swamps and then were oxidized and stacked during the interval of the volcanic eruptions (Figure 17). However, low (C$_{29}$/C$_{27}$)$\alpha\alpha\alpha$-20R sterane values, (C$_{19}$ + C$_{20}$)TT/C$_{23}$TT values, and TAR values indicate a different origin for the deposits from the Jiangbasitao Formation in the well ZBL. Minor amounts of diterpenoid suggest the low contribution of conifers. The high relative abundance of vitrodetrinite and micrinite suggests the presence of plant debris. Given the high water level, the OM may be mainly derived from the terrigenous plant debris which was transported from the nearby island arc via rivers (Figure 17).

In Figure 16, we can find that the depositional environment became more oxidizing from the early Carboniferous to the late Carboniferous. The Pr/Ph values were lower than 1 during the deposition of the Lower Jiangbasitao Formation source rocks, indicating a reducing environment. Low TAR values, (C$_{19}$ + C$_{20}$)TT/C$_{23}$TT, and (C$_{29}$/C$_{27}$)$\alpha\alpha\alpha$-20R sterane values of the Lower Jiangbasitao Formation deposits suggest minor contributions from the higher plants but a major contribution of planktons. Therefore, the accumulation of OM was likely to be controlled by the good preservation conditions and plankton inputs. During the deposition of the Upper Jiangbasitao Formation source rocks, terrigenous plant debris inputs contribute to the accumulation of OM. In the well ZBC, source rocks of the Upper Batamayineishan Formation and the Lower Batamaiyineishan Formation with high TOC values were controlled by the contributions of the higher plants, which can be induced by the higher plant indicators (C$_{29}$/C$_{27}$)$\alpha\alpha\alpha$-20R sterane, (C$_{19}$ + C$_{20}$)TT/C$_{23}$TT, R_{dit}, and TAR.

5.5. Gas and Oil Generation Potential and Implications for Deep Hydrocarbon Exploration. Source rocks in the Shibei Sag have the gas and oil generational potential. Source rocks of the Batamayineishan Formation were mainly composed of carbonaceous mudstones. The high TOC values, moderate maturity, and high HI suggest their good hydrocarbon generation. 30% of the source rocks from the Batamayineishan Formation are type II$_2$−II$_1$ kerogen, suggesting their oil generation potential. The identified resinite, alginate (telalginite and lamalginite), resinite, cutinite, and hydrocarbon-rich vitrinite can contribute to oil generation. As mentioned above, these source rocks of the Batamayineishan Formation were deposited in a swamp environment with a high contribution of terrigenous OM inputs. This suggests that source rocks deposited in the swamp environment may also have a limited liquid hydrocarbon generation. Source rocks in the Jiangbasitao Formation are mainly tuffaceous mudstones which have a fair to good OM richness. They are mainly type III kerogen with the predominant contribution of higher plant inputs which were deposited in a sub-oxic swamp environment, indicating a gas generation potential. However, mudstones in the ZBH area which were deposited in a fluvial/delta environment were poor for hydrocarbon generation.

The condensate oil and gas were discovered in the boreholes in the Triassic and the Carboniferous strata (in the well ZBH), which confirms the possibility of hydrocarbon generation. As discussed above, tuffaceous mudstone in the Jiangbasitao Formation is a set of good gas-prone source rocks. From the seismic profile, we can speculate that there is a thick layer of source rocks in the Jiangbasitao Formation (Figure 3). Based on the burial thermal evolution of the study area (Figure 18), we can find that the bottom source rock of the Jiangbasitao Formation in the Shibei Sag reached a burial depth of about 1300 m and Ro reached 0.5% in the middle of the early

https://doi.org/10.1021/acsearthspacechem.2c00241
ACS Earth Space Chem. 2023, 7, 92−109

Carboniferous (about 330 Ma) and entered the hydrocarbon threshold. In the late early Carboniferous (about 315 Ma), the burial depth reached about 1950 m, the Ro reached 0.7%, and the source rocks entered the main oil generation stage. In the late Carboniferous (about 310 Ma), the burial depth reached about 2650 m, the Ro reached 1.3%, the source rocks entered the gas generation stage, and the source rocks of the Jiangbasitao Formation reached a high-mature to post-mature stage today.

Similar to the Kelameili gas field, the thick tuffaceous mudstones with fair to good OM richness and high maturity combined with the volcanic reservoirs can form a large-scale gas field. Our understanding of the source rocks with high contribution of gymnosperms and pre-gymnosperms is expected to provide new insights into the deep condensate and wet-gas exploration and predictions for the deep exploration in similar basins elsewhere.

6. CONCLUSIONS

The Carboniferous source rocks were deposited during the interval of volcano eruptions. Their hydrocarbon generation potential, genetic type of kerogen, thermal maturity, the origin of OM, and depositional environment were analyzed based on organic petrographic and organic geochemical methods. The conclusions can be reached as follows:

(1) Most samples have fair to excellent source rock richness with good hydrocarbon generation potential. Source rocks from the Jangbasitao Formation contain the type III kerogen (except the samples ZBL-23 and ZBL-24), while the source rocks from the Batamayineishan Formation contain type II_2-III kerogen.

(2) The terrigenous plants are the predominant source for the Carboniferous source rocks. Abundant bicyclic sesquiterpenoids and diterpenoid biomarkers suggest the conifer inputs. The extremely high amounts of phyllocladanes and retene and the lack of simonellite indicate the presence of conifer species of families other than Pinaceae. Pre-gymnosperms predominate pteridophytes during the late Carboniferous period. However, the contributions of algae cannot be ignored, especially in the Lower Jiangbasitao Formation.

(3) The Carboniferous source rocks were deposited under a transitional lacustrine-fluvial/deltaic environment, especially a peat/swamp environment in well ZBB and ZBC areas.

(4) From the early Carboniferous to the late Carboniferous, the environment became more oxic, the water level dropped, and higher plants flourished, especially in the swamp/peats under a dry climate.

(5) The Carboniferous source rocks are already in the oil window, and those in the Jiangbasitao Formation with higher maturity have a good condensate-wet gas generation potential. Given the biological contributions, thermal maturity, and large thickness, the source rocks in the Carboniferous have a good petroleum exploration potential.

ASSOCIATED CONTENT

Supporting Information

The Supporting Information is available free of charge at https://pubs.acs.org/doi/10.1021/acsearthspacechem.2c00241.

Bulk geochemical data (TOC, S_1, S_2, T_{max}, PY, HI, PI, and R_r) of the Carboniferous source rocks from the Shibei Sag, Junggar Basin and EOM contents and $\delta^{13}C$ values of the studied samples (PDF)

AUTHOR INFORMATION

Corresponding Author

Zhihuan Zhang − *State Key Laboratory of Petroleum Resources and Prospecting, China University of Petroleum (Beijing), Beijing 102249, China; College of Geoscience, China University of Petroleum, Beijing 102249, China;* orcid.org/0000-0001-9224-3365; Email: zhangzh3996@vip.163.com

Authors

Xue Chen − *State Key Laboratory of Petroleum Resources and Prospecting, China University of Petroleum (Beijing), Beijing 102249, China; College of Geoscience, China University of Petroleum, Beijing 102249, China*

Xiao Jin − *Development and Research Center, National Geological Archives of China, China Geological Survey, Beijing 100037, China*

Xinjian Zhu − *PetroChina Hangzhou Research Institute of Geology, Hangzhou 310023, China*

Ningning Zhong − *State Key Laboratory of Petroleum Resources and Prospecting, China University of Petroleum (Beijing), Beijing 102249, China; College of Geoscience, China University of Petroleum, Beijing 102249, China*

Complete contact information is available at: https://pubs.acs.org/10.1021/acsearthspacechem.2c00241

Funding

The work presented in this paper was supported by the SINOPEC Shengli Oilfield (China) and the State Key Laboratory of Petroleum Resources and Prospecting, China University of Petroleum (Beijing), Beijing.

Notes

The authors declare no competing financial interest.

ACKNOWLEDGMENTS

We would like to thank the reviewers for their helpful comments, suggestions, and scientific and linguistic revisions of the manuscript. The authors are grateful to SINOPEC Shengli Oilfield (China) for supplying the samples and providing original geological data. In addition, we thank the State Key Laboratory of Petroleum Resources and Prospecting for GC−MS analysis.

ABBREVIATIONS

TOC, total organic carbon; OM, organic matter; Rr, random vitrinite reflectance; C_1j, Jiangbasitao Formation; C_2b, Batamayineishan Formation; T_{max}, temperature of maximum pyrolysis yield; EOM, extractable organic matter; GC−MS, gas chromatography−mass spectrometry; SIM, selective ion monitoring; TIC, total ion current; PDB standard, Pee Dee Belemnite standard; Ro, vitrinite reflectance; HI, hydrogen index; V, vitrodetrinite; M, micrinite; A, alginate; T, telalginite; L, lamalginite; Re, resinite; Fl, fluorinate; Cu, cutinite; I, inertinite; Fu, fusinite; H-V, hydrocarbon-rich vitrinite; PY, production yield; PI, production index; nd, no data; CPI, carbon preference index; TAR, terrestrial aquatic ratio; ETR, extended tricyclic terpane ratio; GI, gammacerane index; TTs, tricyclic

https://doi.org/10.1021/acsearthspacechem.2c00241
ACS Earth Space Chem. 2023, 7, 92−109

terpanes; TeT, tetracyclic terpane; Pr, pristine; Ph, phytane; TS, total sulfur

REFERENCES

(1) Chen, Z.; Wang, X.; Wang, X.; Zhang, Y.; Yang, D.; Tang, Y. Characteristics and petroleum origin of the Carboniferous volcanic rock reservoirs in the Shixi Bulge of Junggar Basin, western China. *Mar. Petrol. Geol.* **2017**, *80*, 517−537.

(2) Sun, P.; Wang, Y.; Leng, K.; Li, H.; Ma, W.; Cao, J. Geochemistry and origin of natural gas in the eastern Junggar Basin, NW China. *Mar. Petrol. Geol.* **2016**, *75*, 240−251.

(3) Tao, K.; Cao, J.; Wang, Y.; Ma, W.; Xiang, B.; Ren, J.; Zhou, N. Geochemistry and origin of natural gas in the petroliferous Mahu sag, northwestern Junggar Basin, NW China: Carboniferous marine and Permian lacustrine gas systems. *Org. Geochem.* **2016**, *100*, 62−79.

(4) Da, J.; Hu, Y.; Zhao, M.; Song, Y.; Xiang, B.; Qin, S. Features of source rocks and hydrocarbon pooling in the Kelameili gasfield, the Junggar Basin. *Oil Gas Geol.* **2010**, *31*, 187−192. (in Chinese)

(5) Xulong, W.; Mengjun, Z.; Baoli, X.; Jiang, D.; Yiqin, J.; Cuimin, L. Carboniferous source rocks in the Ludong-Wucaiwan area, Junggar Basin, NW China. *Petrol. Explor. Dev.* **2010**, *37*, 523−530 (in Chinese).

(6) Gong, D. Y.; Lan, W. F.; Xiang, H.; Ding, J.; Wu, W. A.; Hu, Z. L. Genetic types and origins of natural gases from the eastern Junggar Basin. *J. China Univ. Min. Technol.* **2019**, *48*, 142−152. (in Chinese)

(7) Lai, S. X.; Li, Y. P.; Ning, L. Carboniferous oil and gas exploration breakthrough condition analysis of Di'nan bulge. *Xinjiang Geol.* **2018**, *36*, 490−496. (in Chinese)

(8) Wei, Y.; Chen, G.; Lu, S.; Song, Z.; Qi, R.; Wang, W.; Gong, D.; Wang, F. Re-examination of genetic types and origins of natural gases from Deibei Uplift, eastern Luliang Uplift Junggar Basin. *J. Nat. Gas Geosci.* **2019**, *4*, 257−265 (in Chinese).

(9) Xulong, X.; Mengjun, Z.; Baoli, X.; Jiang, D.; Yiqin, J.; Cuimin, L. Carboniferous source rocks in the Ludong-Wucaiwan area, Junggar Basin, NW China. *Petrol. Explor. Dev.* **2010**, *37*, 523−530 (in Chinese).

(10) Li, E.; Jin, J.; Wang, J.; Luo, Z.; Ma, W.; Mi, J.; He, D.; Wang, M. Source of Carboniferous natural gas in Kelameili area, Junggar Basin. *Nat. Gas Geosci.* **2020**, *31*, 1515−1523 (in Chinese).

(11) Zhang, S.; Ren, B.; Jiang, Y.; Liu, X.; Kang, L. Geochemical characteristics and the origin of natural gas in Carboniferous, Eastern Junggar Basin. *Nat. Gas Geosci.* **2015**, *26*, 1627−1926. (in Chinese)

(12) Yu, S.; Wang, X. L.; Xiang, B. L.; Liao, J. D.; Wang, J.; Li, E. T.; Yan, Y. H.; Cai, T. L.; Zou, Y. R.; Pan, C. C. Organic geochemistry of Carboniferous source rocks and their generated oils from the Eastern Junggar Basin, NW China. *Org. Geochem.* **2014**, *77*, 72−88.

(13) Gong, D.; Song, Y.; Wei, Y.; Liu, C.; Wu, Y.; Zhang, L.; Cui, H. Geochemical characteristics of Carboniferous coaly source rocks and natural gases in the Southeastern Junggar Basin, NW China: Implications for new hydrocarbon explorations. *Int. J. Coal Geol.* **2019**, *202*, 171−189.

(14) Peters, K. E.; Walters, C. C.; Moldowan, J. M.*The Biomarker Guide*; Cambridge University Press: Cambridge, 2005.

(15) Song, Y.; Wang, S.; Fang, D. Formation and evolution of petroleum systems of Junggar Basin. *Acta Pet. Sin.* **2000**, *21*, 20−25.

(16) Zhang, Y.; Zhang, N. Oil/gas enrichment of large superimposed basin in Junggar Basin. *China Pet. Explor.* **2006**, *11*, 59−64.

(17) Pan, Y.; Huang, Z.; Li, T.; Guo, X.; Xu, X.; Chen, X. Environmental response to volcanic activity and its effect on organic matter enrichment in the Permian Lucaogou Formation of the Malang Sag, Santanghu Basin, Northwest China. *Palaeogeogr. Palaeoclimatol. Palaeoecol.* **2020**, *560*, 110024.

(18) Sofer, Z. Stable carbon isotope compositions of crude oils: application to source depositional environments and petroleum alteration. *AAPG Bull.* **1984**, *68*, 31−49.

(19) Silliman, J. E.; Meyers, P. A.; Bourbonniere, R. A.; Bertrand, P.; Eglinton, G. Record of postglacial organic matter delivery and burial in sediments of Lake Ontario. *Org. Geochem.* **1996**, *24*, 463−472.

(20) Peters, K. Guidelines for evaluating petroleum source rock using programmed pyrolysis. *AAPG Bull.* **1986**, *70*, 318−329.

(21) Peters, K. E.; Cassa, M. R.*Applied Source Rock Geochemistry*; AAPG Memoirs, 1994; pp 93−120.

(22) Espitalié, J.; Senga Makadi, K.; Trichet, J. Role of the mineral matrix during kerogen pyrolysis. *Org. Geochem.* **1984**, *6*, 365−382.

(23) Mukhopadhyay, P. K.; Wade, J. A.; Kruge, M. A. Organic facies and maturation of Jurassic/Cretaceous rocks, and possible oil-source rock correlation based on pyrolysis of asphaltenes, Scotian Basin, Canada. *Canada. Org. Geochem.* **1995**, *22*, 85−104.

(24) George, S. C.; Volk, H.; Dutkiewicz, A.; Ridley, J.; Buick, R. Preservation of hydrocarbons and biomarkers in oil trapped inside fluid inclusions for >2 billion years. *Geochim. Cosmochim. Acta* **2008**, *72*, 844−870.

(25) George, S. C.; Ruble, T. E.; Dutkiewicz, A.; Eadington, P. J. Assessing the maturity of oil trapped in fluid inclusions using molecular geochemistry data and visually-determined fluorescence colours. *Appl. Geochem.* **2001**, *16*, 451−473.

(26) Böcker, J.; Littke, R.; Hartkopf-Fröder, C.; Jasper, K.; Schwarzbauer, J. Organic geochemistry of Duckmantian (Pennsylvanian) coals from the Ruhr Basin, western Germany. *Int. J. Coal Geol.* **2013**, *107*, 112−126.

(27) Pickel, W.; Kus, J.; Flores, D.; Kalaitzidis, S.; Christanis, K.; Cardott, B. J.; Misz-Kennan, M.; Rodrigues, S.; Hentschel, A.; Hamor-Vido, M.; Crosdale, P.; Wagner, N. Classification of liptinite - ICCP System 1994. *Int. J. Coal Geol.* **2017**, *169*, 40−61.

(28) Shanmugam, G. Significance of coniferous rain forests and related organic matter in generating commercial quantities of oil, Gippsland Basin, Australia. *AAPG Bull.* **1985**, *69*, 1241−1254.

(29) Powell, T. G. Pristane/phytane ratio as environmental indicator. *Nature* **1988**, *333*, 604.

(30) Izart, A.; Palhol, F.; Gleixner, G.; Elie, M.; Blaise, T.; Suarez-Ruiz, I.; Sachsenhofer, R. F.; Privalov, V. A.; Panova, E. A. Palaeoclimate reconstruction from biomarker geochemistry and stable isotopes of n-alkanes from Carboniferous and Early Permian humic coals and limnic sediments in western and eastern Europe. *Org. Geochem.* **2012**, *43*, 125−149.

(31) Zhang, S.; Wu, S.; Zhang, T.; Cao, C.; Ma, W.; Shi, J.; Sun, G. Organofacies and paleoenvironment of Lower Carboniferous mudstones (Dishuiquan Formation) in Eastern Junggar, NW China. *Int. J. Coal Geol.* **2015**, *150*−*151*, 7−18.

(32) Philp, R. P.; Gilbert, T. D.; Friedrich, J. Bicyclic sesquiterpenoids and diterpenoids in Australian crude oils. *Geochim. Cosmochim. Acta* **1981**, *45*, 1173−1180.

(33) Püttmann, W.; Kalkreuth, W. Comparison of hydrocarbon compositions in a sequence of humic coals, cannel coals and oil shales from the Pictou Coalfield, Nova Scotia. *Atl. Geol.* **1989**, *25*, 93−103.

(34) Raymond, A. C.; Liu, S. Y.; Murchison, D. G.; Taylor, G. H. The influence of microbial degradation and volcanic activity on a Carboniferous wood. *Fuel* **1989**, *68*, 66−73.

(35) Vliex, M.; Hagemann, H. W.; Püttmann, W. Aromatized arborane/fernane hydrocarbons as molecular indicators of floral changes in Upper Carboniferous/Lower Permian strata of the Saar-Nahe Basin, southwestern Germany. *Geochim. Cosmochim. Acta* **1994**, *58*, 4689−4702.

(36) Alexander, R.; Kagi, R. I.; Noble, R. Identification of the bicyclic sesquiterpenes drimane and eudesmane in petroleum. *J. Chem. Soc., Chem. Commun.* **1983**, 226−228.

(37) Auras, S.Variation von Chemofossilien und stabilen Isotopen in Kohlen und Pflanzenresten aus dem Bereich der Westfal/Stefan-Grenze im euramerischen Karbon. Doctoral Dissertation, Johannes Wolfgang Goethe-Universität, Frankfurt am Main, 2004.

(38) Simoneit, B. R. T. Diterpenoid compounds and other lipids in deep-sea sediments and their geochemical significance. *Geochim. Cosmochim. Acta* **1977**, *41*, 463−476.

(39) Simoneit, B. R. T.Cyclic terpenoids of the geosphere. In *Biological Markers in the Sedimentary Record*; Johns, R. B., Ed.; Elsevier: Amsterdam, 1986; pp 43−99.

(40) Grantham, L. J.; Douglas, A. The nature and origin of sesquiterpenoids in some Tertiary fossil resins. *Geochim. Cosmochim. Acta* **1980**, *44*, 1801−1810.

https://doi.org/10.1021/acsearthspacechem.2c00241
ACS Earth Space Chem. 2023, 7, 92−109

(41) Hagemann, H. W.; Hollerbach, A.Relationship between the macropetrographic and organic geochemical composition of lignites. In *Advances in Organic Geochemistry 1979*; Douglas, A. G., Maxwell, J. R., Eds.; Pergamon: Oxford, 1980; pp 631−638.
(42) Noble, R. A.; Alexander, R.; Kagi, R. I.; Knox, J. Tetracyclic diterpenoid hydrocarbons in some Australian coals, sediments and crude oils. *Geochim. Cosmochim. Acta* **1985**, *49*, 2141−2147.
(43) Dev, S.Terpenoids. In *Natural Products of Woody Plants*; Rowe, J. W., Ed.; Springer: Berlin, 1989; Vol. *1*, pp 691−807.
(44) Otto, A.; Walther, H.; Püttmann, W. Sesqui- and diterpenoid biomarkers preserved in Taxodium-rich Oligocene oxbow lake clays, Weisselster basin, Germany. *Org. Geochem.* **1997**, *26*, 105−115.
(45) Otto, A.; Wilde, V. Sesqui-, di-, and triterpenoids as chemosystematic markers in extant conifers-A review. *Bot. Rev.* **2001**, *67*, 141−238.
(46) Haberer, R. M.; Mangelsdorf, K.; Wilkes, H.; Horsfield, B. Occurrence and palaeoenvironmental significance of aromatic hydrocarbon biomarkers in Oligocene sediments from the Mallik 5L-38 Gas Hydrate Production Research Well (Canada). *Org. Geochem.* **2006**, *37*, 519−538.
(47) Schulze, T.; Michaelis, W. Structure and origin of terpenoid hydrocarbons in some German coals. *Org. Geochem.* **1990**, *16*, 1051−1058.
(48) Fleck, S.Corrélation entre Géochimie Organique, Sédimentologie et Stratigraphie Séquentielle pour la Caractérisation des Paléoenvironnements de Dépôt. PhD Thesis, Université Henri Poincaré, Nancy, France, 2001; Vol. *387*.
(49) Peters, K. E.; Moldowan, J. M.*The Biomarker Guide: Interpreting Molecular Fossils in Petroleum and Ancient Sediments*; Prentice Hall: Englewood Cliffs, NJ, 1993.
(50) Waples, D. W.; Machihara, T. M.Biomarkers for Geologists. *AAPG Methods in Exploration Series No. 9*; American Association of Petroleum Geologists: Tulsa, Oklahoma, 1991.
(51) Tao, S.; Wang, C.; Du, J.; Liu, L.; Chen, Z. Geochemical application of tricyclic and tetracyclic terpanes biomarkers in crude oils of NW China. *Mar. Petrol. Geol.* **2015**, *67*, 460−467.
(52) Hao, F.; Zhou, X. H.; Zhu, Y. M.; Yang, Y. Y. Mechanisms for oil depletion and enrichment on the Shijiutuo uplift, Bohai Bay Basin, China. *Bull. Am. Assoc. Pet. Geol.* **2009**, *93*, 1015−1037.
(53) Huang, W.-Y.; Meinschein, W. G. Sterols as ecological indicators. *Geochem. Cosmochim. Acta* **1979**, *43*, 739−745.
(54) Moldowan, J. M.; Sundararaman, P.; Schoell, M. Sensitivity of biomarker properties to depositional environment and/or source input in the Lower Toarcian of SW-Germany. *Org. Geochem.* **1986**, *10*, 915−926.
(55) Ma, L.; Zhang, Y.; Zhang, Z.; Zhang, G.; Wang, S. The geochemical characteristics of the Fengcheng Formation source rocks from the Halaalate area, Junggar Basin, China. *J. Petrol. Sci. Eng.* **2020**, *184*, 106561.
(56) Xu, H.; George, S. C.; Hou, D. Algal-derived polycyclic aromatic hydrocarbons in Paleogene lacustrine sediments from the Dongying Depression, Bohai Bay Basin, China. *Mar. Petrol. Geol.* **2019**, *102*, 402−425.
(57) Liu, B.; Bechtel, A.; Sachsenhofer, R. F.; Gross, D.; Gratzer, R.; Chen, X. Depositional environment of oil shale within the second member of Permian Lucaogou Formation in the Santanghu Basin, Northwest China. *Int. J. Coal Geol.* **2017**, *175*, 10−25.
(58) Wang, C.; Wang, Q. X.; Chen, G. J.; He, L.; Xu, Y.; Chen, L. Y.; Chen, D. F. Petrographic and geochemical characteristics of the lacustrine black shales from the Upper Triassic Yanchang Formation of the Ordos Basin, China: implications for the organic matter accumulation. *Mar. Pet. Geol.* **2017**, *86*, 52−65.
(59) Li, Q.; Wu, S. H.; Xia, D. L.; You, X. L.; Zhang, H. M.; Lu, H. Major and trace element geochemistry of the lacustrine organic-rich shales from the Upper Triassic Chang 7 Member in the southwestern Ordos Basin, China: Implications for paleoenvironment and organic matter accumulation. *Mar. Pet. Geol.* **2020**, *111*, 852−867.
(60) Zhang, K.; Liu, R.; Liu, Z. J.; Li, B. L.; Han, J. B.; Zhao, K. Influence of volcanic and hydrothermal activity on organic matter enrichment in the Upper Triassic Yanchang Formation, southern Ordos Basin, Central China. *Mar. Pet. Geol.* **2020**, *112*, 104059.
(61) Radke, M.; Welte, D. H.; Willsch, H. Distribution of alkylated aromatic hydrocarbons and dibenzothiophenes in rocks of the Upper Rhine Graben. *Chem. Geol.* **1991**, *93*, 325−341.
(62) Wilkin, R. T.; Barnes, H. L.; Brantley, S. L. The size distribution of framboidal pyrite in modern sediments: an indicator of redox conditions. *Geochim. Cosmochim. Acta* **1996**, *60*, 3897−3912.
(63) Song, J.; Littke, R.; Weniger, P. Organic geochemistry of the lower Toarcian Posidonia Shale in NW Europe. *Org. Geochem.* **2017**, *106*, 76−92.
(64) Rullkötter, J.; Littke, R.; Schaefer, R. G.Characterization of Organic Matter in Sulfur-Rich Lacustrine Sediments of Miocene Age (Nördlinger Ries, Southern Germany). In *Geochemistry of Sulfur in Fossil Fuels*; Orr, W. L., White, C. M., Eds.; ACS Symposium Series; ACS Publications, 1990; Vol. *429*, pp 149−169.
(65) Grohmann, S.; Romero-Sarmiento, M. F.; Nader, F. H.; Baudin, F.; Littke, R. Geochemical and petrographic investigation of Triassic and Late Miocene organic-rich intervals from onshore Cyprus, Eastern Mediterranean. *Int. J. Coal Geol.* **2019**, *209*, 94−116.
(66) Hughes, W. B.; Holba, A. G.; Dzou, L. I. P. The ratios of dibenzothiophene to phenanthrene and pristane to phytane as indicators of depositional environment and lithology of petroleum source rocks. *Geochim. Cosmochim. Acta* **1995**, *59*, 3581−3598.
(67) Kara-Gülbay, R.; Sen, Ö.; Korkmaz, S.; Demirel, İ. H. Lower Karboniferous shales in the Eastern Tauride Belt, southern Turkey: source rock characteristics. *J. Pet. Geol.* **2014**, *37*, 25−42.
(68) Xiao, H.; Li, M. J.; Yang, Z.; Zhu, Z. L. Distribution patterns and geochemical implications of C19−C23 tricyclic terpanes in source rocks and crude oils occurring in various depositional environments. *Geochimica* **2019**, *48*, 161−170.

https://doi.org/10.1021/acsearthspacechem.2c00241
ACS Earth Space Chem. 2023, 7, 92−109